2023 International Materials Selection Challenge Final Reports

Curated by the Ansys Academic Development Team and the Ansys Academic Field Team

education@ansys.com

Summary

This resource collects the reports of the finalist projects of the Ansys International Material Selection Challenge. These projects were submitted by student teams from universities in Brazil, Egypt and Spain. Each proposal was supervised by a professor and reviewed by members of the Ansys Academic Program before being presented in front of a jury composed of Prof. Elena Maria Tejado Garrido (UPM, Spain), Sara Onrubia Garcia (Ansys Spain), Prof. Julio Cesar Dutra (Centro Universitário FEI, Brazil), Prof. Jean-Dominique Guérin (Université Polytechnique des Hauts de France, France) and Prof. Germán Alcalá Penadés (UCM, Spain). The final presentations were held at the Moncloa Campus of the Polytechnic University of Madrid on November 8th, 2023.

The project reports collected here are meant to serve as inspiration for students and educators working on material selection projects. They span a broad range of applications and industries, such as civil engineering, consumer products, bioengineering, energy generation and aerospace. They demonstrate how Ansys Granta EduPack can foster innovation and optimal product designs, with examples using many of its tools as well as other Ansys simulation software.

Table of Contents

Fishing Nets from Sustainable Natural Materials

The American University of Cairo, Cairo, Egypt

Supervisor: Dr. Mahmoud Farag

Students: Aliaa Moussa, Heidi Mohamed, Mariam El Halabi

Report Contents

1. Summary

Egypt produces 1.2 million tonnes of banana crop every year, and the market exhibits an annual growth rate of 5.49% [1]. However, The pseudo-stem of the banana tree has to be cut off every year in order for a new crop to grow [2].Therefore, banana tree waste is very abundant in Egypt, around 1.8 million tonnes are produced annually [3]. Additionally, the disposal methods that are currently used in practice include burning the stems or throwing them in lakes, which causes immense environmental pollution [4]. The fibers extracted from the pseudostem are of very high quality and can be utilized in industrial applications such as textiles [2]. In El-Bahtiny village, which is located in El-Ismailia, Egypt by the Suez Canal, fishermen have started abandoning their craft and their homes due to the lack of local affordable fishing gear. The imported materials used for manufacturing fishing nets have increased in price due to the ongoing economic crisis in Egypt and fishermen can no longer afford it. As a result, cheaper, locally-produced sustainable banana-fiber fishing nets are being proposed. The Ansys Granta Edupack was used to evaluate the proposed hypothesis and compare banana fibers to the traditionally used silk and polymeric fibers, as well as to other natural fibers. The advanced level (level 3) of the simulation tool was used for the comparison. All material families were considered at the beginning, then the tree tool was used to narrow down the selection. The limit tool was also used to eliminate materials of very low strength. Since a cheaper price is one of the main selling points of the sustainable fishing nets, all charts were plotted to show the variation of a property with respect to its price across all candidate materials. The properties considered in the analysis were: price/kg, density, specific strength, elongation percentage, young's modulus, durability in freshwater, durability in sea water, CO2 footprint in production, biodegradability and renewable content. Humidity absorption at saturation was also studied for the banana fibers. Banana fibers were concluded to be acceptable for the application of fishing nets, after certain treatments are carried out to enhance its permeability.

2. Objectives

a. Carry out a market study in the village of El-Bahtiny to test the community's willingness to use the new fishing nets and the women's ability and acceptance to weave the product.
b. Develop a preliminary prototype of the banana fibers fishing net, to determine the needed modifications for the product.
c. Compare the banana fibers properties, such as strength, cost and eco cost, against other natural, like jute and flax, and synthetic materials and select the optimum fibers for our application.
d. Design and infographic to showcase the advantages of using natural materials in the new fishing nets.
e. Determine the processing needed to improve the performance of the new nets.

3. Problem statement

El-Bahtiny is a fishermen's village that is located on the Suez Canal, near El-Ismailia city, by the Temsah Lake in Egypt [see Appendix (A)]. The fishing craft, which is the main livelihood of this community, is currently shrinking due to the scarcity and increasing prices of imported fishing net materials caused by the Egyptian Government's restrictions on imported goods and devaluation of the Egyptian Pound.

4. Proposed solution

Provide the fishing community of the El-Bahtiny village with a local, sustainable, and affordable material for the manufacturing of fishing nets. Using natural biodegradable materials for the fishing nets can avoid shedding microplastics and reduce the risk to marine life caused by the currently used synthetic plastics which are responsible for the ghost nets phenomenon [5]. The project also aims to fulfill SDGs 8, 12, and 14 by providing decent work opportunities to the villagers by involving women in the manufacturing process and providing fishermen with the necessary fishing equipment to continue working. Locating a production hub for sustainable fishing nets in El-Bahtiny could also help attract ecotourism to the village.

5. Results and conclusions

Interviews were carried out with the fishermen to test their readiness to start using a new sustainable and local material [see Appendix (A)]. The fishermen are aware of the negative impacts that nylon ghost nets have on the number of fish in the sea, where synthetic nets get stuck in rocks for hundreds of years, and destroy the eggs laid down by the fish on the sea bed.

Moreover, interviews were carried out with the women of El-Bahtiny village in order to test their ability to use the new proposed material. The women were enthusiastic about the project and wanted to start working right away, so it was decided that alongside the net-weaving tasks, they would help create other merchandise to upcycle the banana fibers into valuable products [see Appendix (A)].

A preliminary prototype was made by fishermen in Egypt using the banana fibers before any processing [see Appendix (B)]. The fisherman was reluctant to do. The fisherman's final feedback was that the material is very strong; however, it needs to be woven into a continuous strand of yarn to be easier to work with. Hence, a continuous yarn of banana fiber was produced using the same manufacturing process used for flax; a summary of the manufacturing process is provided in Appendix (E).

The initial screening was done using the tree tool to limit material families to silk, natural and polymeric fibers. As Nylon-6 is the most commonly used for manufacturing the fishing nets utilized by the community of El-Bahtiny, its properties were used as a reference. The limit tool was used to eliminate

all materials with specific strength lower than 526 KPa/Kg, which is the minimum shown by Nylon-6 [see Figure (1)]. Human hair and wool fibers were eliminated for being unfit for the intended function. Specific strength is used because it is crucial that the weight of the fishing net is as light as possible. Banana Fiber displays the highest specific strength in all natural fibers [Figure (2)]. It is also cheaper than all the polymeric candidates and than 50% of the natural fibers [Figure (2)]. The range of variation of its specific strength is narrow, which supports its use in industrial applications [Figure (2)]. Banana fiber also has excellent biodegradability, where it is the third most biodegradable fiber after palm and silk [Figure (3)]. However, palm showed relatively low specific strength which does not make it the best material choice for fishing nets [Figure (2)]. The CO2 footprint is the lowest amongst all fibers which further proves that it is a sustainable material [Figure (4)]. Silk has the highest production CO2 footprint [Figure (4)], therefore its use in making fishing nets should also be reduced to help reduce the fishing craft's environmental impact. The density of banana fibers is slightly higher than Nylon-6, but lower than many of the natural fibers [Figure (5)]. Banana fiber has a moderate elasticity compared to the rest of the candidates [Figure (6)], but it is significantly higher than nylon-6, which makes banana fiber easier to weave into nets. However, the elongation percentage of banana fiber is too low [Figure (7)], which is expected for all natural fibers. Durability of banana fiber is acceptable in both fresh and saltwater [Figures (8) & (9)]. However, it is worth noting that the durability of Nylon-6 is graded as excellent in both media. Lastly, there is a visible discrepancy in Figure (10) between the percentage of renewable content of natural fibers and polymeric fibers, with an exception for PLA because it is extracted from renewable sources such as corn starch, while other polymers are extracted from fossil fuels [6].

It was observed from the database on the software that the humidity absorption level of banana fibers needs improvement: where banana fibers absorb 8.5-10% of the humidity at saturation, while Nylon-6 absorbs only 4-4.5%. Accordingly, the fibers need to undergo a water repellent treatment by coating with a hydrophobic material before the fibers are woven into strands. Experimental data found in literature have shown that water absorbency of banana-fiber composites could be decreased by 32% though an alkali treatment and again by 63% through water treatment by immersing the fiber in perfluoroalkyl acrylate copolymer [7].

Banana fiber showed good performance considering its price, specific strength, young's modulus, CO2 footprint in production, biodegradability and renewable content. However, It is expected that the new nets would be heavier compared to the nylon nets of the same size, unless a hybrid fiber is created by mixing banana fiber with a low-density natural fiber like Kenaf. Kenaf Fibers showed an overall good performance with the expectation of having a large range in specific strength. Decreasing the permeability of the fiber will increase its durability in fresh and salt water, which need improvement to perform as well as Nylon-6. The low elongation percentage is another disadvantage that was concluded for the fiber, which should be closely studied as it may hinder the manufacturing process of the fiber.

6. References

[1] “Egypt bananas production, 1961-2022,” Knoema, https://knoema.com/atlas/Egypt/topics/Agriculture/Crops-Production-Quantity-tonnes/Bananas-production

[2] Balda, Sanjeev & Sharma, Aarjoo & Capalash, Neena & Sharma, Prince. (2021). Banana fibre: a natural and sustainable bioresource for eco-friendly applications. Clean Technologies and Environmental Policy. 23. 10.1007/s10098-021-02041-y.

[3] Use of banana wastes as hay or silage for feeding ruminants, https://jappmu.journals.ekb.eg/article_119386_afebf372c2fbf05cc6b8a2331c4141ee.pdf

[4] Mostafa, Marwan & Uddin, Nasim. (2016). Experimental Analysis of Compressed Earth Block (CEB) with Banana Fibers Resisting Flexural and Compression Forces. Case Studies in Construction Materials. 5. 10.1016/j.cscm.2016.07.001.

[5] L. Hancock, “Our Oceans are haunted by ghost nets: Why that’s scary and what we can do,” WWF, https://www.worldwildlife.org/stories/our-oceans-are-haunted-by-ghost-nets-why-that-s-scary-and-what-we-can-do--25

[6] “What is pla? (everything you need to know),” TWI, https://www.twi-global.com/technical-knowledge/faqs/what-is-pla#:~:text=Polylactic%20acid%2C%20also%20known%20as,distillation%20and%20polymerization%20of%20petroleum.

[7] K. Z. M. A. Motaleb, A. Ahad, G. Laureckiene, and R. Milasius, “Innovative banana fiber nonwoven reinforced polymer composites: Pre- and post-treatment effects on physical and mechanical properties,” Polymers, https://www.ncbi.nlm.nih.gov/pmc/articles/PMC8588415/

7. Appendices

Appendix (A): El-Bahtiny Community





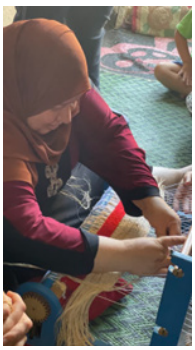

Appendix (B): Preliminary Prototype

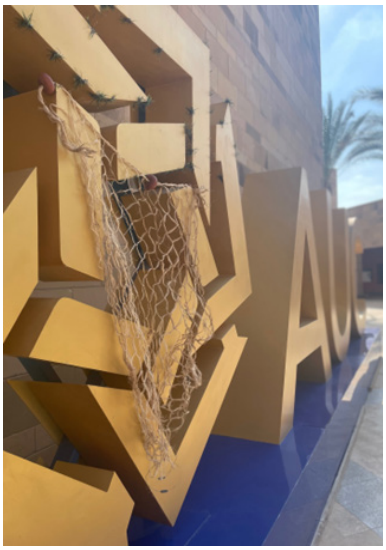

Appendix (C): Charts & Screening Results

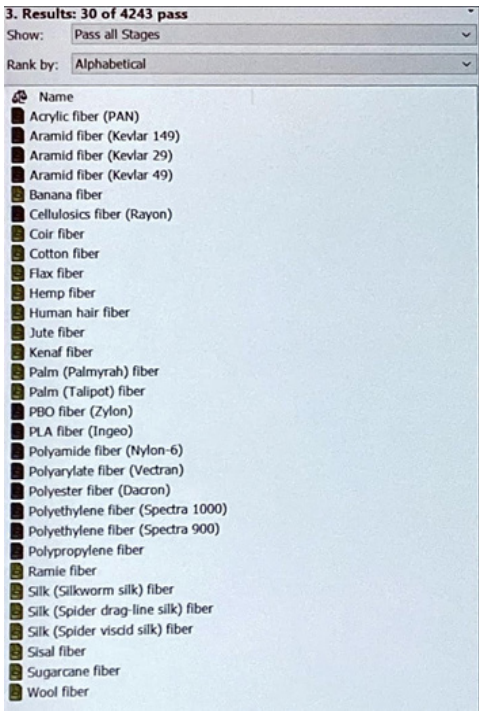

Figure (1): All possible material candidates

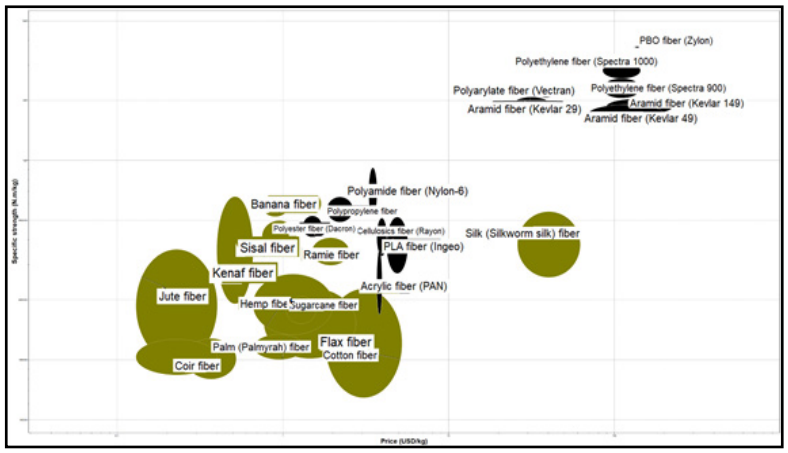

Figure (2): Specific Strength of Candidate Materials Against

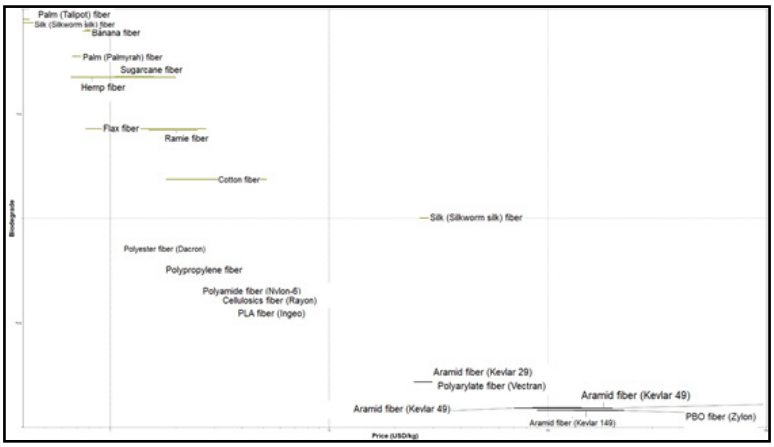

Figure (3): Biodegradability of Candidate Materials Against Price

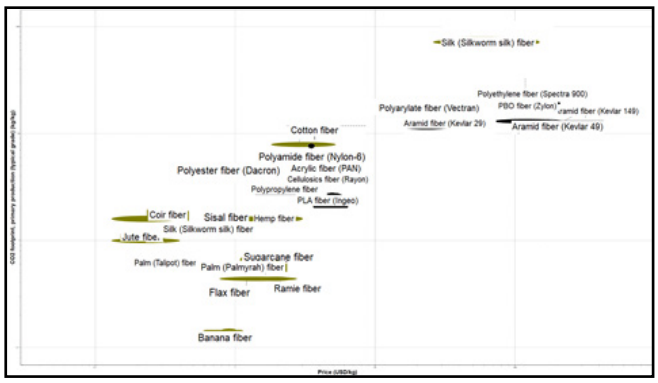

Figure (4): CO2 Footprint of Candidate Materials

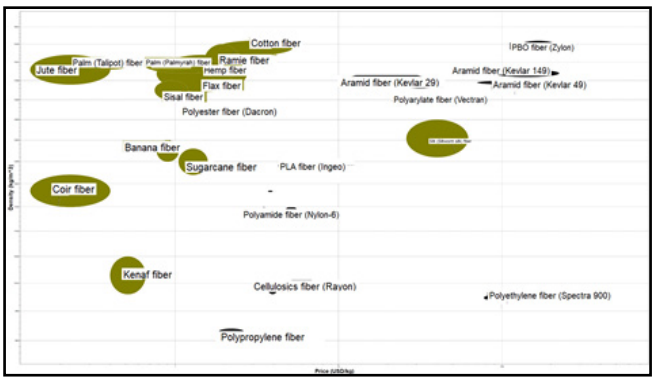

Figure (5): Density of Candidate Materials Against Price

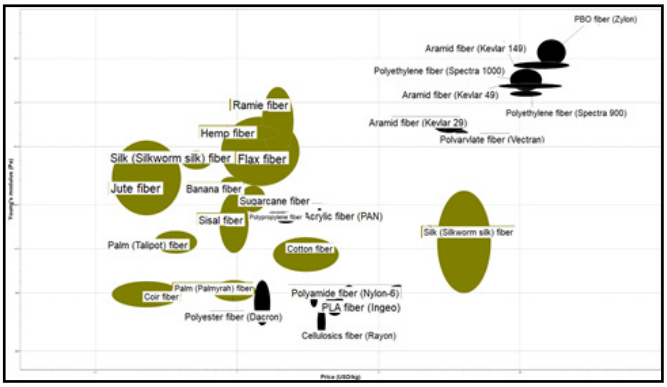

Figure (6): Elasticity of Candidate Materials Against Price

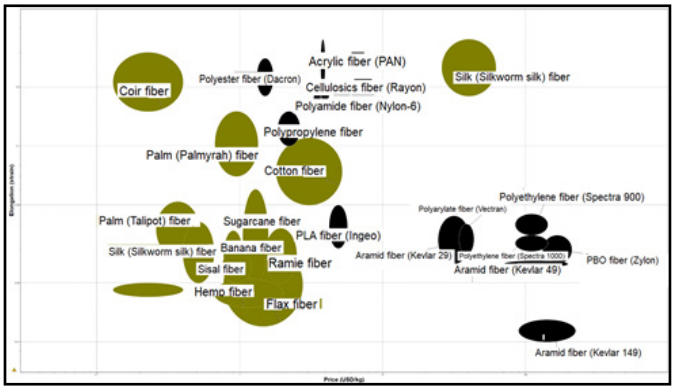

Figure (7): Elongation Percentage of Candidate Materials Against Price

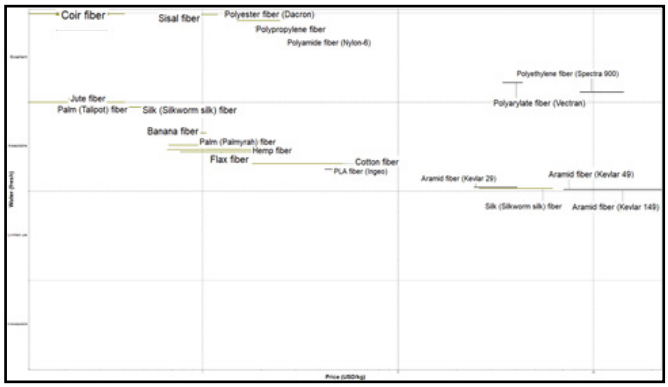

Figure (8): Durability in Fresh Water of Candidate Materials Against

Figure (9): Durability in Salt Water of Candidate Materials Against Price

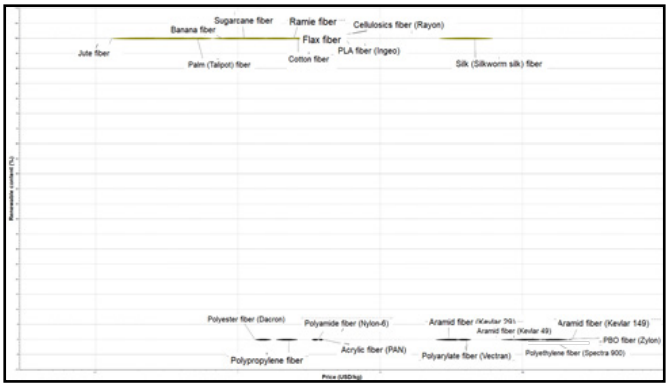

Figure (10): Percentage of Renewable Content of Natural and Synthetic Materials vs Price

Appendix (D): Infographic

An Infographic was designed to show the community the benefits of using the banana fiber nets over the traditionally-used materials. This English version is provided for ease of access, however, another Arabic version will be distributed amongst fishermen.

Appendix (E): Fibers Manufacturing process

In order to incorporate the fisherman's feedback that the fibers should be continuous, two spools of yarn were produced at a flax manufacturing plant located in Tanta, Egypt. The top spool is 100% banana fiber, while the bottom is a hybrid material containing both banana fiber and flax. The same machinery and manufacturing process employed for flax was used, which is as follows:

1. The fiber is submerged in water for 1 day (Retting)
2. Fibers are left to dry in the sun (Drying)
3. The fibers are drawn over combs and pass over 3 stages (Hackling)
4. Fibers pass over metal pins to separate them into grouped continuous strands (Drawing).
5. The strands are twined and collected in spools (Spinning)

Reduced Environmental Impact and Enhanced Performance: A Study of Materials for Bamboo Bicycle Frame Joints

Federal University of Paraná, Lactec Curitiba, Brazil

Supervisors: Carlo Giuseppe Filippin, Lucas Gomes Fonçatti

Student/s: Tiago Chelni, Gilberto Suss Neto

Report Contents

1. Summary

The design of a bamboo bicycle frame stands out for its use of bamboo poles as part of the tubular structure. This choice is justified by the ease of obtaining bamboo in tropical and subtropical regions, as well as its naturally suitable shape for the purpose. A notable example of application is the socio-environmental project Ghana Bamboo Bikes Initiative, which provides income for families in rural areas of Ghana through the production and sale of these bicycles. Typically, in the manufacturing process, the tubes are joined using fibers and resin through a manual process in which the fibers are bundled, soaked in resin, and wrapped at the joints. After the composite has dried, the artisan performs finishing touches through sanding and painting. However, it is possible to enhance the manufacturing process by replacing the resin and fiber joints with pre-fabricated connections. By exploring different materials for these joints, such as metals, natural materials, and composites with a polymer matrix containing natural or synthetic fibers, artisans can achieve technological advancements in bamboo bicycles. In this context, the objective of this study is to select materials that offer a high ratio of strength, stiffness, and density while minimizing costs and environmental impact. The authors discuss the possibility of using these various materials in the joints to enhance the design of bamboo bicycle frames. This approach will enable more efficient manufacturing with improved performance while maintaining the sustainable and cost-effective characteristics of bamboo usage. The study aims to contribute to the evolution of bamboo bicycles, making them more accessible, durable, and environmentally friendly

2. Objectives

The purpose of this project is to conduct a comparative analysis of various materials used in the manufacturing of bicycles, exploring the universe of materials with the aim of identifying viable solutions for connections in bamboo bicycles and subsequently determining the most suitable material. In this context, the material selection should meet the following objectives:

I. Screen the materials;
II. Ensure that the connection is lightweight, strong, and has enough stiffness
III. Ensure that the chosen material has a low carbon footprint and embodied energy;
IV. Finally, verify that the selected material exhibits satisfactory structural performance through simulations in a virtual prototype.

3. Problem statement

There is a universe of possibilities for bicycle frame materials. However, the most commonly used ones are steel, aluminum, carbon fiber, and titanium (1). A less explored option is bamboo. In these frames, connections are frequently constructed utilizing a combination of natural or synthetic fibers and epoxy resin (2,3). Alternatively, pre-fabricated connections of metal tubes can be found, such as those used in the Bicycle Schools project in the municipality of São Paulo (4).

Choosing the best material for connections in a bamboo frame requires establishing design considerations such as boundary conditions and an understanding of existing mechanical behaviors. In terms of boundary conditions, a bicycle frame comprises two reaction points, one at each wheel, and a load on the seat, handlebars, and crank set. In terms of mechanical behavior, the existing loads generate stresses in the vertical, horizontal, and diagonal tubes, assigning them functions of columns and beams (5).

However, ensuring proper design considerations is not enough; it is also essential to take environmental requirements into account. As discussed by Agyekum (6) in his work, social and environmental impacts on a community in Ghana that manufactures bamboo bicycles are assessed. The author indicates that the overall environmental impact of bamboo is about 50% lower than that of aluminum and approximately 30% lower than that of steel frames. According to Ashby (5), materials and energy are integrated into a complex system with significant interactions.
Finally, the project must ensure that the material choice is safe for the cyclist. This is crucial because the joints of bicycle tubes are sensitive points in the design (7,8), and in accordance with standards such as ASTM F2711-19 (9) or NBR14714 (10), bicycles must establish safety and strength requirements for the user.

4. Proposed solution

The first step of the selection process will be the screening of the universe of materials, focusing on comparing the most commonly used materials in bicycle frames, plus bamboo. The screening is delimited by the properties of these materials, which include price, density, Young's modulus, and maximum yield stress. In addition to applying these limits, the screening is limited to studying the following material families: natural composites, PCB laminate, polymer matrix, ferrous metals, non-ferrous metals, natural wood, and wood-like materials.

In the second stage, the strategy proposed by Ashby (5) for the case of multiple constraints is employed. Therefore, the design requirements are defined as follows:

Function: Tubular Joints for Bamboo Bicycles.
Constraint:

Strength - the joint must not fail due to beam loading effects (horizontal tubes), or column loading effects (vertical tubes).

Stiffness - the joint should be sufficiently stiff to prevent high displacements when the bicycle is loaded.

Length and radius.

Objectives: Minimize mass.
Free Variables: Material selection and thickness.

From the development of EQUATIONS 1, material indices are obtained. It is possible to observe that for both beam and column loading conditions, the indices for stiffness constraints are the same. The same applies to strength constraints. Therefore, we proceed to work with just one bubble chart using the Chart/Select tool in Granta Ansys EduPack (11). With the set of EQUATIONS 2, linking constants are obtained, which are used in comparing the individual performance of materials.

The third stage involves evaluating environmental impacts on embodied energy and carbon footprint during the most impactful phase of the product life cycle, which focuses on the raw material production phase. For this stage, the Eco Audit tool from Granta Ansys EduPack (11) is used for assessment.

The final stage consists of structural verification. For this purpose, three different geometries for bicycle frames were modeled, considering the specific characteristics of the materials. Tubular joints were used for external metallic connections to the tubes, laminated joints for external synthetic composites to the tubes, and cylindrical joints of laminated bamboo for internal fittings to the tubes. Carbon fiber connections were treated as surfaces and modeled in Ansys ACP, while the remaining connections and bamboo tubes were treated as solids and surfaces, respectively. A static structural analysis, following the methodology of Covill (7), was conducted for the condition of a cyclist pedaling while seated and standing on the bicycle.

5. Results and conclusions

For the screening process, the following materials were chosen as representatives of each family: AISI 4130 annealed steel (12), Aluminum 6061 T6 wrought (13), Epoxy/HS carbon fiber resin-infused woven biaxial lay-up (14), Ti-3Al-2.5V Grade 9 (15), and Bamboo. TABLE 1 presents the main evaluated properties. Based on these properties, the last row presents the limit values used in the screening. By applying the property limits and material families, the selection was narrowed down to 996 materials. For the analysis of multiple constraints, the graphs in FIGURE 1 and FIGURE 2 were obtained based on the Material Indices from EQUATIONS 1. The linking constants, C_{cv} for beam loads and C_{cc} for column loads (EQUATIONS 2), are positioned on the right side of the graph in FIGURE 1. Therefore, it can be deduced that the density-to-stiffness ratio dominates among the materials analyzed. As a result, to minimize mass, only the materials within the envelope, whose vertex is on the C_{cc} coupling line, are considered. Thus, FIGURE 2 is obtained, in which it is possible to observe the candidate materials in more detail.

For the material that will have the best performance in both criteria, strength, and stiffness, the masses m_1 and m_2 are equated (EQUATIONS 2). The values of M_1 and M_2 are obtained for each material (TABLE 2) from FIGURE 2, estimated values for application conditions (TABLE 3), and F/L^2 are isolated to obtain the performance for the structural loading coefficient of each material, see connection lines for

$(F/(L^2))_v$ and $(F/(L^2))_c$ in FIGURE 2. As the best option, the Epoxy/HS carbon fiber composite (24.52MPa; 27.58MPa) appears first, while AISI 4130 steel appears with the lowest performance (7.73MPa; 8.69MPa). Therefore, bamboo shows satisfactory performance among typical frame materials.

FIGURE 3 presents the results obtained through the Eco Audit in Granta Ansys EduPack (11). The most significant impacts are observed in the material acquisition phase. Ti-3Al-2.5V (Grade 9) is the material that exhibits the worst results, with 900.0 MJ of embodied energy and a CO_2 footprint of 52.0 $kg_{CO2}/kg_{material}$. Epoxy/HS carbon fiber, a common material used in joints, showed the second-worst performance, with 440 MJ of embodied energy and a CO2 footprint of 31.0 $kg_{CO2}/kg_{material}$. Aluminum 6061 T6 showed a performance like Epoxy/HS carbon fiber, while AISI 4130 steel performed better, with 61.0 MJ of embodied energy and a CO_2 footprint of 4.5 $kg_{CO2}/kg_{material}$. Bamboo demonstrated the best performance of all for applications, with 15.0 MJ of embodied energy and a CO_2 footprint of 0.2 $kg_{CO2}/kg_{material}$. FIGURE 3 also illustrates the potential of some materials when recycled or reused, with a focus on metallic materials. However, recycling metallic connections may become less attractive when resin and bamboo are incorporated.

The present analysis, of a static structural nature, focused on simulating the behavior of the Epoxy/HS composite with carbon fibers and AISI 4130 annealed steel, as they exhibited extreme performance in FIGURE 2. In addition to their wide applicability in bicycle frames. Bamboo, considered as an alternative replacement, was also considered. The results obtained, as shown in TABLE 4, provide a comprehensive view of the maximum stresses observed in the simulations of the connections and the maximum deformations occurring in the bicycle frame structure.

FIGURE 4 presents the results for deformations and stresses for the bamboo frame, with maximum stresses reaching 111.33 MPa. This is acceptable depending on the bamboo species. For example, for Phyllostachys aurea bamboo, traditionally used by artisans, the maximum stress is around 193.10 - 288.00 MPa (16). Therefore, in both analyzed situations, pedaling while seated or standing, bamboo exhibited low von-Mises stresses for the connection structure. Special attention should be given to changes in sections which showed stress peaks.

Consequently, it is plausible to conclude that bamboo meets the mechanical requirements of strength, stiffness, and density, as corroborated by the data presented in the bubble chart in FIGURE 2 and TABLE 4. Furthermore, it is important to highlight that bamboo emerged as the most environmentally responsible choice among the alternatives subjected to analysis, as illustrated in FIGURE 3.

6. References

1. Norman P. Bike frame materials compared: alloy vs carbon vs steel vs titanium - BikeRadar [Internet]. 2021 [cited 2023 Sep 3]. Available from: https://www.bikeradar.com/advice/buyers-guides/bike-frame-materials/
2. Art Bike Bamboo Klaus Volkmann [Internet]. 2023 [cited 2023 Sep 3]. Available from: https://www.artbikebamboo.com.br/
3. Bamboocycles [Internet]. 2023 [cited 2023 Sep 3]. Available from: https://bamboocycles.com/
4. Escolas de Bicicleta - Prefeitura da Cidade de São Paulo [Internet]. 2012 [cited 2023 Sep 3]. Available from: https://www.prefeitura.sp.gov.br/cidade/secretarias/comunicacao/noticias/?p=106905
5. Ashby M. Materials Selection in Mechanical Design. Elsevier, editor. Rio de Janeiro; 2013.
6. Agyekum EO, Fortuin K, Van Der Harst E. Environmental and social life cycle assessment of bamboo bicycle frames made in Ghana. 2016 [cited 2023 Sep 4]; Available from: http://dx.doi.org/10.1016/j.jclepro.2016.12.012
7. Covill D, Allard P, Drouet JM, Emerson N. An Assessment of Bicycle Frame Behaviour under Various Load Conditions Using Numerical Simulations. Procedia Eng. 2016 Jan 1;147:665–70.
8. Tomaszewski T. Fatigue life analysis of steel bicycle frame according to ISO 4210. Eng Fail Anal [Internet]. 2021 [cited 2023 Sep 28];122:105195. Available from: https://doi.org/10.1016/j.engfailanal.2020.105195
9. F2711 Standard Test Methods for Bicycle Frames [Internet]. [cited 2023 Sep 28]. Available from: https://www.astm.org/f2711-19.html
10. ABNT NBR 14714 NBR14714 Veículo de duas rodas — Bicicleta — Quadro e [Internet]. [cited 2023 Sep 28]. Available from: https://www.target.com.br/produtos/normas-tecnicas/31542/nbr14714-veiculo-de-duas-rodas-bicicleta-quadro-e-garfo-rigido-requisitos-de-seguranca
11. Ansys Granta EduPack. 2022.
12. World Material: SAE AISI 4130 Chromoly Steel, Alloy Material Properties, Chemical Composition [Internet]. 2022 [cited 2023 Sep 11]. Available from: https://www.theworldmaterial.com/sae-aisi-4130-chromoly-steel-alloy-material/
13. Chalco Aluminum: 6061 T6 Aluminum Tube for Bike Frame [Internet]. 2022 [cited 2023 Sep 11]. Available from: https://www.chalcoaluminum.com/knowledge/6061-bicycle-frame-tube/
14. Overholt Z. Bikerumor: Dare Bikes combine OEM experience, new Toray HS-HMC carbon fiber tech, + rim/disc brakes for VSR road bike [Internet]. 2016 [cited 2023 Sep 11]. Available from: https://bikerumor.com/dare-bikes-combine-oem-experience-new-toray-hs-hmc-carbon-fiber-tech-rimdisc-brakes-vsr-road-bike/
15. YUNCH: Grade9 Ti-3al-2.5v Seamless Titanium Tube for Bicycle Manufacturers and Suppliers - Factory Direct Wholesale [Internet]. 2022 [cited 2023 Sep 11]. Available from: https://www.yunchtitanium.com/grade9-ti-3al-2-5v-seamless-titanium-tube-for
16. Vasata ACDP. Análise das propriedades estáticas e dinâmicas das espécies de Bambu bambusa tuldoides e Phyllostachys aurea [Internet]. 2020 [cited 2023 Oct 3]. Available from: http://repositorio.utfpr.edu.br/jspui/handle/1/5228

7. Appendix

TABLE 1: REPRESENTATIVE MATERIALS FOR BICYCLE FRAMES, USED AS REFERENCES FOR SCREENING THE MATERIAL UNIVERSE. (Source Ansys Granta EduPack (11))

Materials	*Price [BRL/kg]*	*Density [kg/m³]*	*Young's modulus [GPa]*	*Yield strength [MPa]*
AISI 4130 annealed	4.10 - 5.42	7.8e3 - 7.9e3	201.0 - 216.0	360.0 - 460.0
Aluminum, 6061, T6, wrought	10.5 - 12.0	2.69e3 - 2.73e3	66.6 - 70.0	240.0 - 280.0
Epoxy/HS carbon fiber, resin infused woven, biaxial lay-up	90.8 – 105.0	1.49e3 - 1.54e3	58.0 - 64.0	533.0 - 774.0
Ti-3Al-2.5V (Grade 9)	118.0 - 145.2	4.47e3 - 4.49e3	91.0 - 95.0	483.0 - 620.0
Bamboo	6.92 - 10.40	600.0 - 800.0	15.0 - 20.0	35.9 – 43.9
Limites	5 - 130	500 - 8e3	10- 210	40 - 700

TABLE 2 – MATERIAL INDICES.(Source: authors)

Materials	M_1	M_2
AISI 4130 annealed	19.7	36.0
Aluminum, 6061, T6, wrought	10.3	40.7
Epoxy/HS carbon fiber, resin infused woven, biaxial lay-up	2.4	25.5
Ti-3Al-2.5V (Grade 9)	8.2	47.8
Bamboo	16.7	25.5

TABLE 3 – ESTIMATED VALUES FOR APPLICATION IN THE BICYCLE.(Source: authors)

Physical quantity	*Unit*	*Value*
Stiffness	K [kN/m]	941.8
Section Length	L [m]	0.2
Load Distribution Constant	C_1	3
Tube Radius	r [mm]	25.0
Beam Length	l [m]	0.6

TABLE 4 – RESULTS FOR MAXIMUM VON-MISES EQUIVALENT STRESSES IN CONNECTIONS AND MAXIMUM DEFORMATIONS.(Source: authors)

	Equivalent von-Mises Stress [MPa]					*Deformation max. [mm]*
	Head Tube	*Seat stays*	*Medium seat tube*	*Botton Bracker*	*Dropo-uts*	
AISI 4130 annealed – Climbing in the saddle	50.09	8.48	21.82	40.45	49.07	2.11
AISI 4130 annealed – Climbing out of the saddle	73.76	23.30	30.80	82.47	76.00	4.53
Epoxy/HS carbon fiber – Climbing in the saddle	38.94	9.11	7.49	13.23	10.74	2.37
Epoxy/HS carbon f. – Climbing out of the saddle	39.25	32.92	43.86	48.70	65.69	4.15
Bamboo – Climbing in the saddle	58.89	19.6	25.15	28.10	12.42	4.15
Bamboo – Climbing out of the saddle	111.33	71.42	60.15	62.13	21.16	9.40

EQUATIONS 1 - SET OF EQUATIONS FOR MATERIAL INDICES.

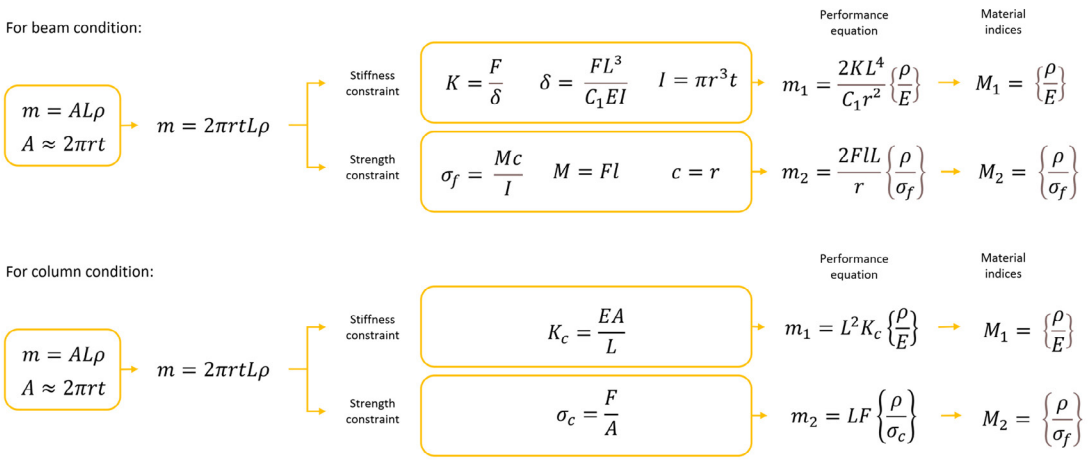

EQUATIONS 2 - SET OF EQUATIONS FOR LINKING CONSTANT.

For beam condition:

$$m_2 = m_1$$

$$M_2 = \left\{\frac{FlC_1 r}{KL^3}\right\} M_1$$

$$C_{cv} = \left\{\frac{FlC_1 r}{KL^3}\right\}$$

For column condition:

$$m_2 = m_1$$

$$M_2 = \left\{\frac{LK_c}{F}\right\} M_1$$

$$C_{cc} = \left\{\frac{LK_c}{F}\right\}$$

$$M_2 = C_c M_1$$

$$\log M_2 = \log M_1 + \log C_c$$

FIGURE 1 - CHART FOR MULTIPLE CONSTRAINTS DENSITY/YIELD STRESS X DENSITY/STIFFNESS, FOR ALL MATERIALS THAT PASSED THE SCREENING.

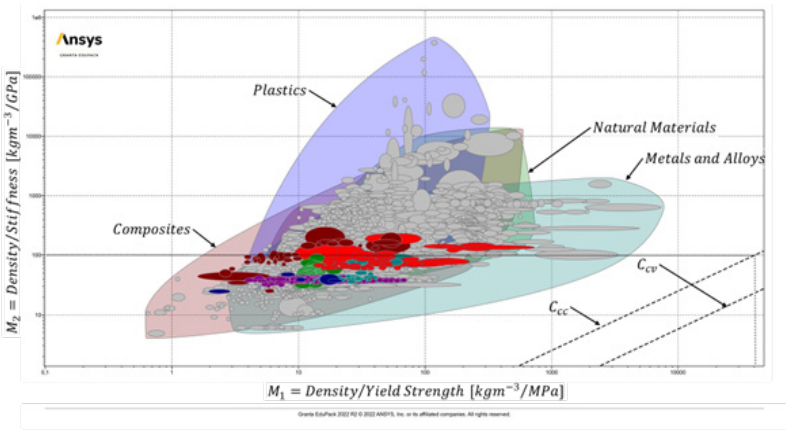

FIGURE 2 - CHART FOR MULTIPLE CONSTRAINTS DENSITY/YIELD STRESS X DENSITY/STIFFNESS, FOCUSING ON THE COMPARED MATERIALS.

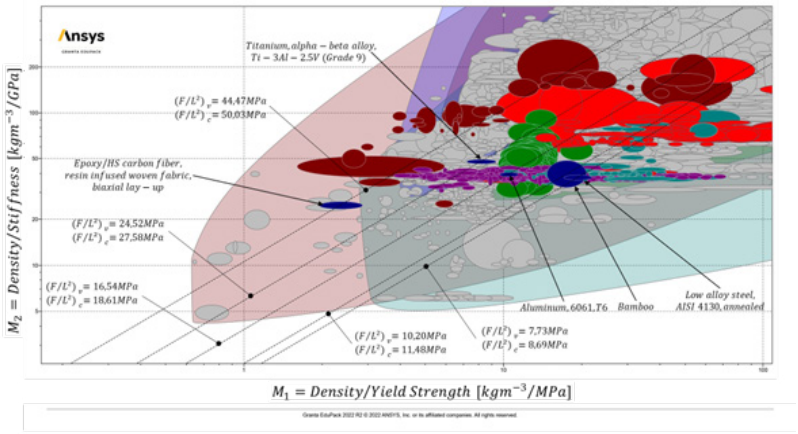

FIGURE 3 - ECO AUDIT ANALYSIS FOR CANDIDATE MATERIALS FOR BAMBOO BICYCLE JOINTS.

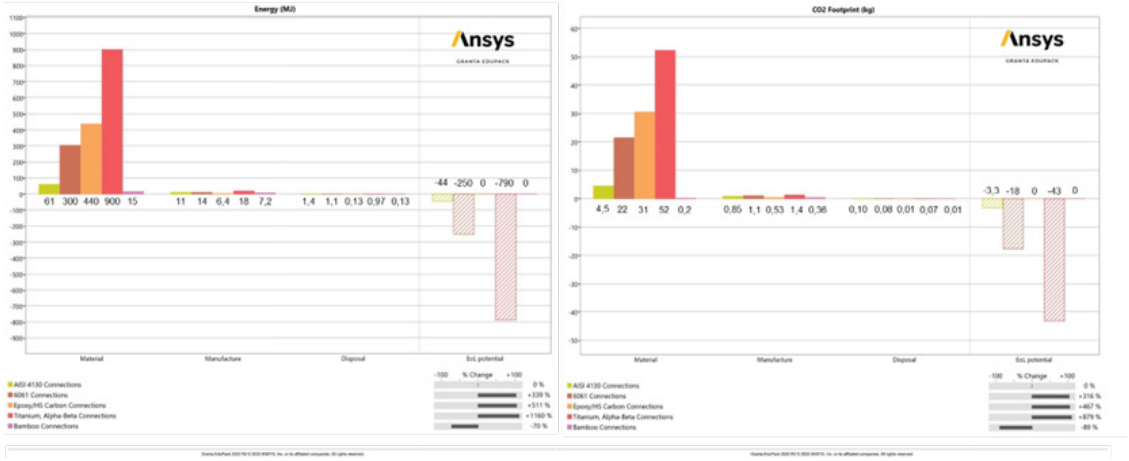

FIGURE 4 - RESULTS OF TOTAL DEFORMATIONS AND VON-MISES STRESSES FOR THE VIRTUAL PROTOTYPING OF A BAMBOO BICYCLE FRAME.

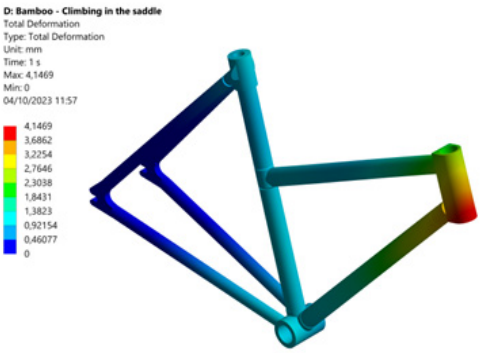

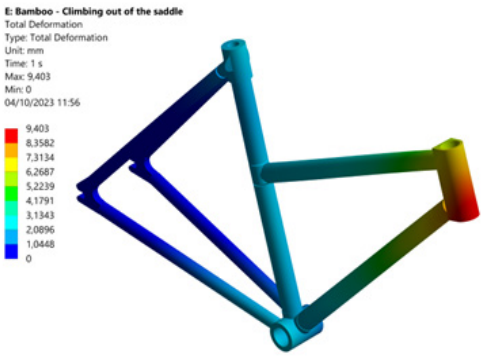

(A) - TOTAL DEFORMATION – CLIMBING IN THE SADDLE. *(B) - TOTAL DEFORMATION – CLIMBING OUT THE SADDLE*

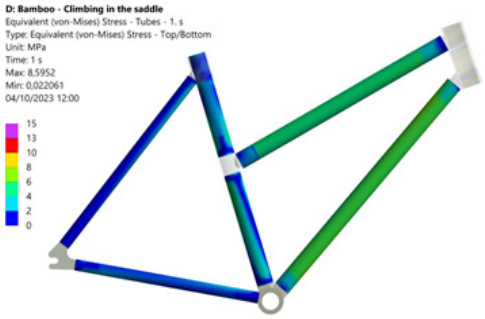

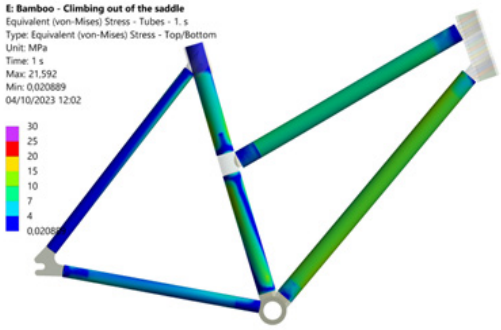

(C) – EQUIVALENT STRESS TUBES – CLIMBING IN THE SADDLE

(D) – EQUIVALENT STRESS TUBES – CLIMBING OUT THE SADDLE

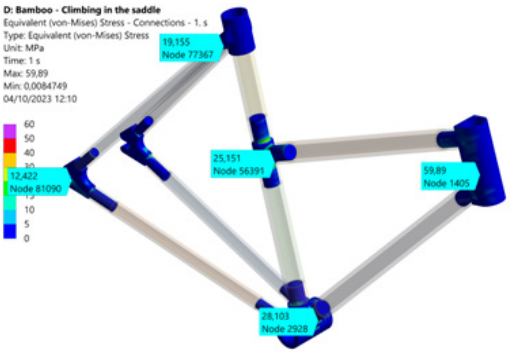

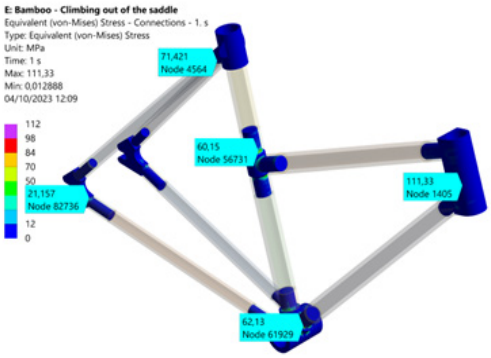

(E) – EQUIVALENT STRESS CONNECTIONS – CLIMBING IN THE SADDLE

(F) – EQUIVALENT STRESS CONNECTIONS – CLIMBING OUT THE SADDLE

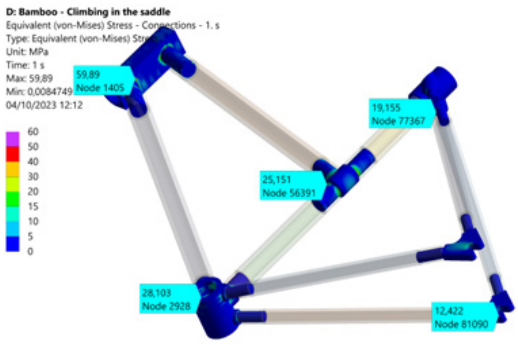

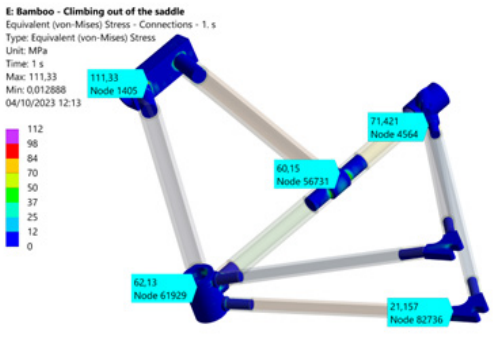

(G) – EQUIVALENT STRESS CONNECTIONS – CLIMBING IN THE SADDLE

(H) – EQUIVALENT STRESS CONNECTIONS – CLIMBING OUT THE SADDLE

Selection of hind leg prosthesis materials for cougars (Puma concolor)

University of Campinas, Campinas, Brazil

Supervisor: Josué Labaki

Student/s: Breno Rocha Coelho, Gustavo Fernandes da Silva, Júlia de Almeida Cobra

Report Contents

1. Abstract

According to the Corredor da Onças Institute[1], there has been a rising trend in the number of roadkills involving wild animals, and it is believed that the actual figures may be even higher. The Puma-Concolor plays a vital role in the ecosystem as a predator in various habitats, and the increasing loss of its members due to these accidents has had a detrimental impact on its population. This situation calls for an adaptation to ensure the surviving individuals can return to the wild, thereby perpetuating the species. With this issue in mind, our project focuses on conducting a comprehensive study and material selection to identify the suitable components for a cougar prosthetic.

To carry out this intricate investigation, we utilized the Ansys Granta Edupack software, which provides access to various advanced and conventional materials. This software allows us to create and assess Ashby Diagrams, enabling us to establish connections between essential parameters and the most appropriate material choices for the desired prosthetic model. Additionally, we made use of the Eco Audit and Synthesizer tools, both valuable resources for evaluating the environmental impact of the project and simulating cost and mechanical properties, respectively.

2. Objectives

With the help of Ansys Granta EduPack software, we aim to select materials for the development of a prosthesis that meets the predatory needs of cougars affected by loss of limbs, providing not only safety, but a new life for the animal in its natural habitat. In addition, the project seeks to define a material that meets the requirements throughout the animal's life, reducing the need for maintenance or replacement of the prosthesis.

3. Problem statement

Ranging from southern Argentina to Canada [2], cougars (Puma concolor) prove to be versatile predators, since they can run fast, swim, and climb rough terrain in their hunt. Despite their widespread presence, road traffic, hunting and deforestation pose a threat to cougar populations, due to the fact that individual losses are harmful to the entire cougar communities, because of their slow reproduction rate. Additionally, because cougars are apex predators, entire ecosystems are affected by fluctuations in the cougar population.

Road traffic is a particular problem, since the expansion of urban areas in cougar habitat results in vehicle traffic crossing cougar hunting grounds, which often results in death or dismemberment of these animals. In the Metro Campinas region in southern Brazil, where our team is located, an average of 25 cougars per kilometer of highway have been run over by cars in the past 10 years [1]. The actual number may be much higher, since most of such accidents are not reported. Several initiatives are underway to mitigate this problem, including safe animal crossings and rehabilitation programs for the wounded animals. This project focuses on the latter initiative, aiming to provide prosthetic limbs to aid in the rehabilitation of cougars.

The restrictive needs of this species in terms of their required physical performance, as a predator, set many challenges in producing academic research. Cougars can weigh between 30-100kg and run up to 80km/h, which are good indicators of the extreme conditions that their bodies must resist. A single leg of a cougar must not only attend to environmental demands such as being waterproof, but also be able to store significant amounts of elastic potential energy, and absorb high values of impact energy in the order of 24,4 kJ without fracturing. Furthermore, since the animal will be reintroduced in nature, the prosthetic limb has to be not only durable over time, under the multiple cyclic forces the limbs will be exposed to, but also be able to endure all the mechanical loads that the animals are subjected to during their lives.

4. Proposed solution

In general, the main mechanical efforts exerted by felines involve activities such as jumping and running, which puts extreme stress on their paw joints as they apply significant force against the ground [3]. These movements occur in two phases: the propulsion or support stage and the recovery or aerial phase. During the first phase, the animal experiences the reaction force of the ground and during the second phase, the forces acting are mainly of gravitational nature. This combination of loading and release subjects the limbs of the animal to fatigue loading.
Additionally, the resulting force or its magnitude varies according to the type of movement, whether it's walking, running, trotting, or galloping.

Based on this analysis, an initial geometry for a prosthetic hind leg for a cougar is proposed. The geometry consists of a blade (Figure 1), designed to maximize the use of stored potential energy during the impulse phase. For this geometry, we used biomimicry to make the movement of the animal more

natural, considering the stress distribution of the anatomy of the hind limb of the animal. To achieve our goal, the material must be lightweight, highly elastic, and impact-resistant at high speeds to expend less energy during the movement and reduce pressure on the knee joints, contributing to metabolic balance.

Using Ansys Mechanical software, we confirmed the distribution of stress throughout the structure through a static analysis using isotropic and anisotropic models (Ansys ACP) with a vertical load of 1 kN (Figure 2). The results shows a maximum stress of 103.25 MPa and a safety factor of 1.5 that was used as a project parameter (Figure 3).

We used Ansys Granta to create comparative material property graphs in order to select the most suitable material for the project. In an initial screening stage, water immersion resistance, toughness and fatigue resistance filters were applied, and then a graph relating toughness and fatigue resistance was plotted to visualize the mechanical constraints and minimum requirements (150 MPa of fatigue strength and 24,4 kJ of toughness defined by the project parameters) (Figure 4 and 5). In a first selection stage, considering the two objectives of mass minimization and of maximization of stored elastic energy in a strength limited design (Equations 1 and 3) we can see by the plots (Figure 6 and 7) that sisal fiber and composite materials specially GFRP and CFRP (Carbon Fiber Reinforced Polymers and Glass Fiber Reinforced Polymers) maximize our performance metrics. In the second selection stage, a diagram was developed associating specific fatigue resistance and fracture toughness with the aim of maximizing fracture toughness with minimum mass (Equation 2)(Figure 8), in which the coupled lines method was applied [4], forming a selection zone in the lower left corner of the graph, where we selected the top twenty materials. Therefore, as the final criterion for classification among these twenty materials, the cost per unit fracture toughness was considered and three desired materials were obtained: sisal fiber, Epoxy/E-glass fiber/UD prepreg, UD lay-up and PEEK/IM carbon fiber/UD prepreg, UD lay-up (Figure 9).

In order to meet the stiffness requirement of the prosthesis, the Synthesizer tool was used to understand the properties of a sisal fiber composite combined with various matrices, which were selected after applying a trade-off curve (Equation 6) (2600 $/kg estimated exchange constant) in a diagram associating specific compressive strength (Equation 4) and specific fracture toughness (Equation 2) (Figures 10 and 11) with the objective of getting the best compromise between both material properties. Finally, analyzing the tensile strength per density we concluded that sisal fiber composites performed worse when compared to PEEK carbon fiber, reducing the reliability of this material, since the prosthesis is designed for high speed impacts and intense continuous cyclic loads (Figure 12). In addition, the PEEK carbon fiber is already used in the orthopedic environment, on account of its bone-like properties [5], but with lower mass and density. After these considerations, one can conclude PEEK carbon fiber is the best material. For the environmental and ecological analysis, using Granta's Eco Audit (Figures 13 and 14) it was estimated a mass of about 900 g for the final product. The prosthesis has a lifespan of at least 10 years, given that it would be a lifelong prosthesis for the adult animal. With these considerations it was possible to conclude from the eco audit analysis that the influence of transportation and manufacturing is negligible when related to the environmental impacts associated with material production (Figure 15), which represents the largest share, and its disposal. In terms of energy and carbon emissions per year of use, in that order, the prosthesis presents 73,8 MJ/year and 5.12 kg/year.

The proposed manufacturing method is vacuum infusion, which considering the rays of the prosthesis geometry is extremely viable. Using this manufacturing method, we used the Synthesizer Part Cost Estimator tool to estimate that the prosthetic leg for cougars would cost 1215 $.

5. Results and conclusions

After a series of tests and considerations, where the Ansys Granta EduPack tools were essential, such as fatigue resistance by fracture toughness, stored elastic energy per unit mass, and fatigue resistance per unit mass, we found that PEEK carbon fiber properties (Figure 16) are the best material to build prosthetic legs for cougars. This is due to its mechanical properties, especially when it comes to its strength and fatigue properties, which are a main concern in this project.

6. References

[1] Número de animais silvestres mortos por atropelamento cresce no inverno 2016, accessed 06 October 2023, <https://g1.globo.com/sp/campinas-regiao/noticia/2016/08/numero-de-animais-silvestres-mortos-por-atropelamento-cr
esce-no-inverno.html>

[2] AZEVEDO, Fernanda Cavalcanti et al. Avaliação do risco de extinção da Onça-parda Puma concolor (Linnaeus, 1771) no Brasil. Biodiversidade Brasileira, [S. l.], p. 107-121, 21 jun. 2013.

[3] Sheila Patek, Andrew Biewener, Animal Locomotion 2018, Oxford University Press, USA

[4] ASHBY, Michael. Seleção de materiais no projeto mecânico. 2019. 5th ed. Editora LTC, Brazil

[5] Kurtz SM, Devine JN. PEEK biomaterials in trauma, orthopedic, and spinal implants. Biomaterials. 2007;28(32):4845-4869

7. Appendix

Equations

(1) $M_1 = \frac{\rho}{\sigma_e}$ (2) $M_2 = \frac{\rho}{K_{1c}}$ (3) $M_3 = \frac{\rho E}{\sigma_c^2}$ (4) $M_4 = \frac{\rho}{\sigma_c}$ (5) $M_5 = \frac{\rho}{\sigma_y}$ (6) $Z = \sum \alpha_i P_i$

Figures

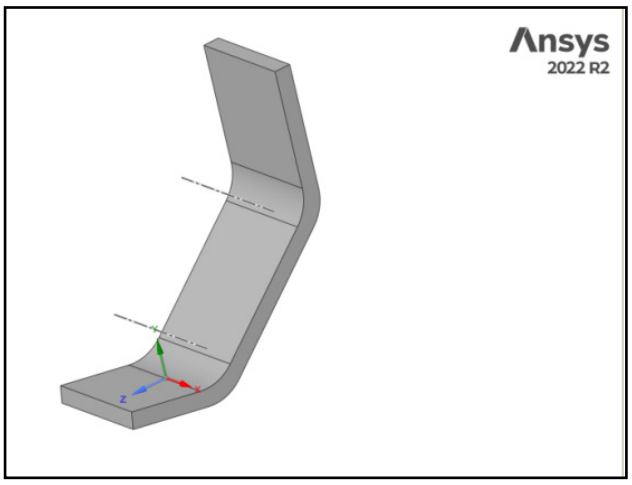

Figure 1: Final geometry of the prosthesis: Authorial.

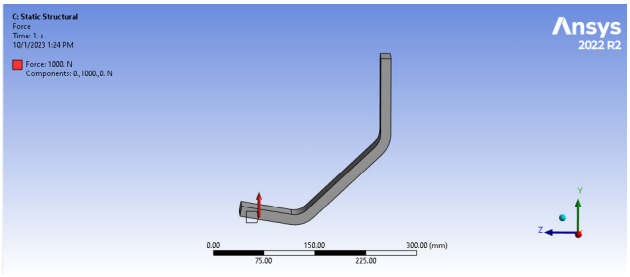

Figure 2: Boundary conditions: Authorial.

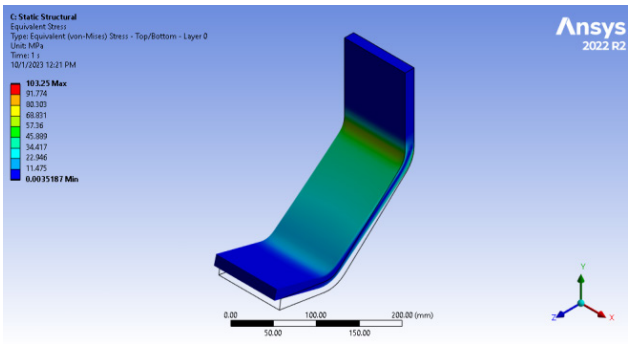

Figure 3: Static simulation results and stress distribution: Authorial.

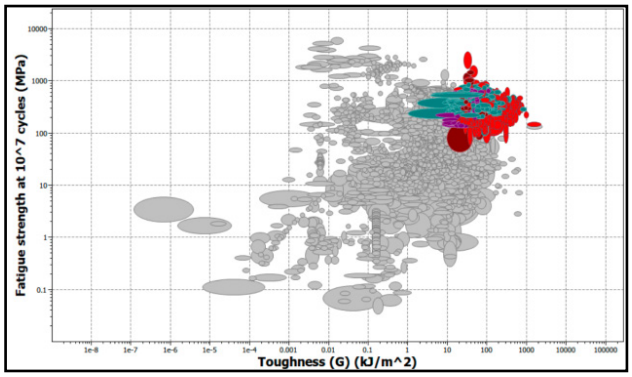

Figure 4: Fatigue resistance versus toughness graph, with gray bubbles symbolizing materials that did not meet the minimum requirements: Authorial.

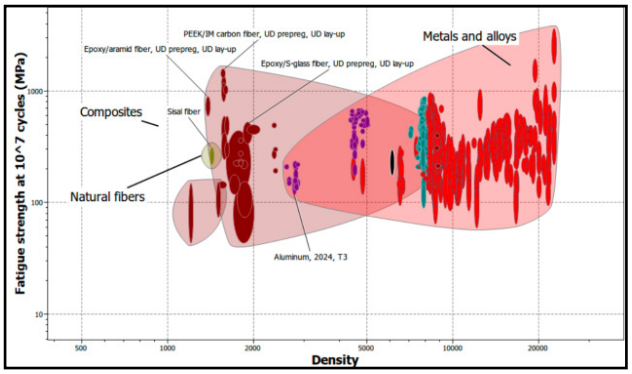

Figure 5: Zooming in on the materials that passed through the initial filtering stage as shown in Figure 4: Authorial.

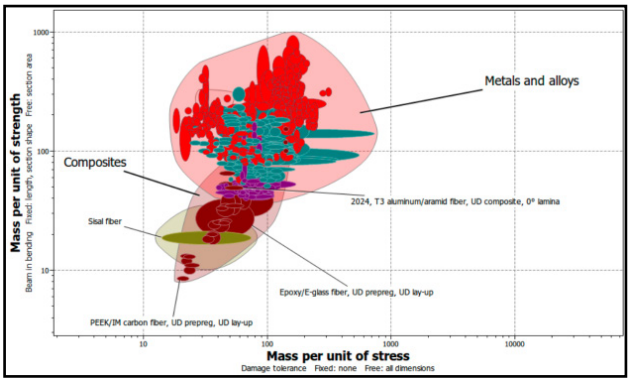

Figure 6: Graph of fatigue resistance per unit mass against fracture toughness per unit mass: Authorial.

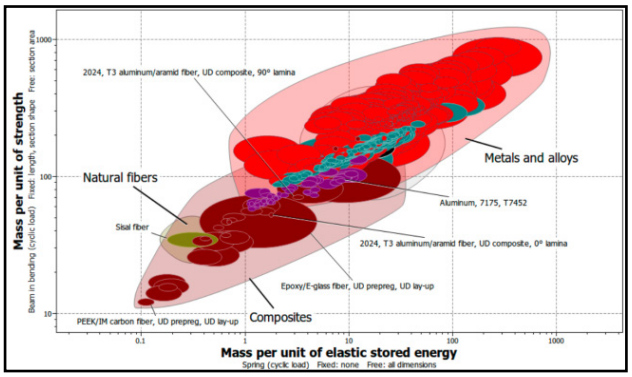

Figure 7: Graph of specific fatigue strength versus specific stored elastic energy: Authorial.

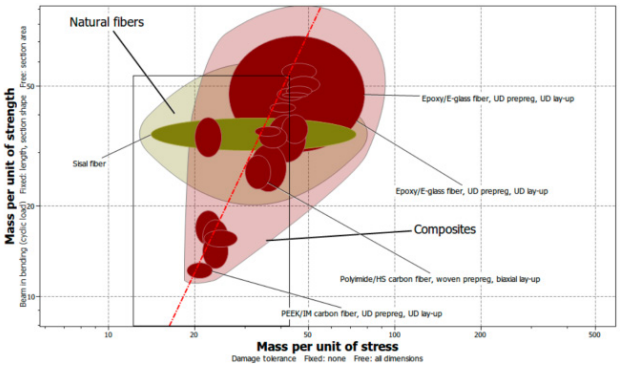

Figure 8: Graph of specific fatigue strength versus fracture toughness, where the red line represents the coupling line between the material indices: Authorial.

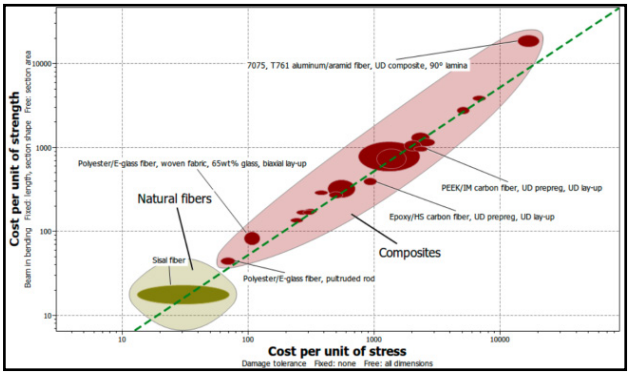

Figure 9: Graph of cost per unit of fatigue strength versus cost per unit fracture toughness, where the green line represents the coupling line between the material indices: Authorial.

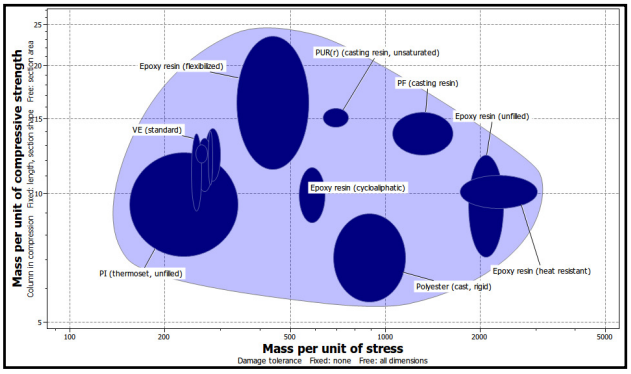

Figure 10: Graph relating specific compressive strength and specific toughness: Authorial.

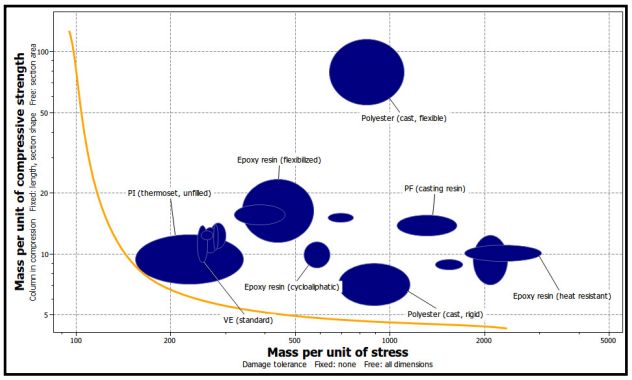

Figure 11: Previous figure with a trade-off curve relating specific fracture toughness (equation 2) and specific compressive strength (equation 4): Authorial.

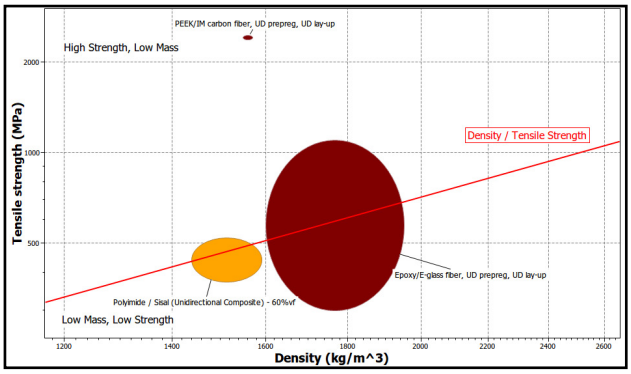

Figure 12: Graph comparing PEEK carbon fiber, Epoxy E-glass and a Polyimide sisal composites: Authorial.

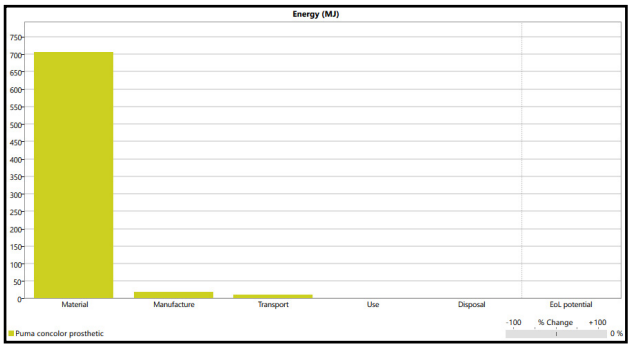

Figure 13: Graph from Eco Audit Report. Energy waste: Authorial.

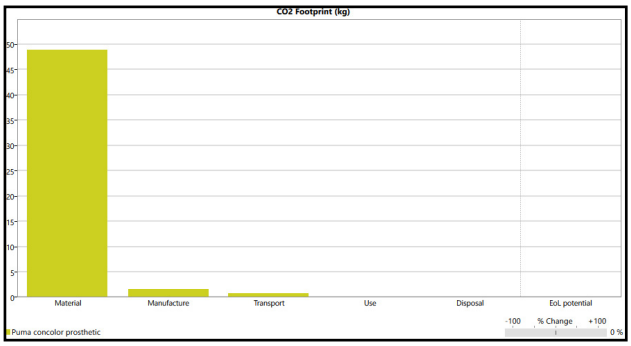

Figure 14: Graph from Eco Audit Report. CO2 footprint: Authorial.

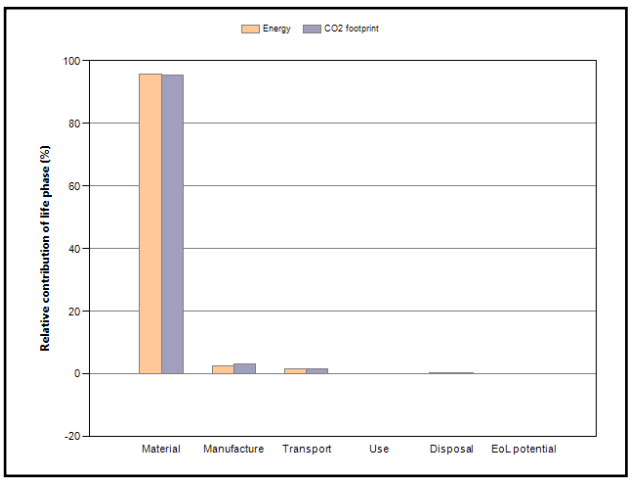

Figure 15: Graph from Eco Audit Report. Relative properties of the PEEK carbon fiber: Authorial.

Mechanical properties

Young's modulus	146	-	149	GPa
Specific stiffness	93.5	-	95.6	MN.m/kg
Yield strength (elastic limit)	2.41e3	-	2.43e3	MPa
Tensile strength	2.41e3	-	2.43e3	MPa
Specific strength	1.54e3	-	1.56e3	kN.m/kg
Elongation	1.36	-	1.81	% strain
Compressive modulus	134	-	148	GPa
Compressive strength	945	-	1.2e3	MPa
Flexural modulus	148	-	150	GPa
Flexural strength (modulus of rupture)	* 2.41e3	-	2.43e3	MPa
Shear modulus	5.4	-	5.5	GPa
Bulk modulus	* 14.8	-	16.3	GPa
Poisson's ratio	0.342	-	0.372	
Shape factor	6.3			
Hardness - Vickers	* 26.1	-	28.5	HV
Hardness - Rockwell M	* 95	-	105	
Hardness - Rockwell R	* 119	-	131	
Elastic stored energy (springs)	1.96e4	-	2.01e4	kJ/m^3
Fatigue strength at 10^7 cycles	* 1.33e3	-	1.58e3	MPa

Figure 16: PEEK carbon fiber important properties: Ansys Granta Database.

Facade scaffolding to contain accidents in civil construction

University of Campinas, Campinas, Brasil

Supervisor: Josué Labaki

Student/s: Gabriel Henrique da Silva, Gustavo dos Santos Magalhães,

Matheus de Lucena Facione Pereira

Table of Contents

1. Summary

A study in 2017 revealed that insufficient scaffolding stability, weak/defective planking and overloading were a few of the main causes in construction site fatal accidents[1]. Approaching these matters from a technical standpoint is a first step to tackling the unsafe environment issues involved in construction jobs. Therefore, this study offers a solution to improve work conditions while also seizing this opportunity to take a more environmentally friendly and cheaper route to scaffolding materials.

The software's tools are used to conduct an in-depth material selection study for the development of a lightweight, durable, resistant, and eco-friendly scaffold that is technically functional, safe and has a longer lifespan. Key considerations will include reducing overall mass and electrical conductivity, enhancing corrosion resistance, incorporating recycled materials, and ensuring the ongoing safe operation of this vital structure within the global construction industry.

To select the material, we employed the Ansys Granta Edu pack software, which provides access to a wide range of advanced and conventional materials. This allowed us to create and evaluate Ashby diagrams with the purpose of correlating essential parameters for selecting the most suitable material for our objective. The selection prioritized selecting a sustainable material that would have a positive socioeconomic impact. To achieve this, we utilized Eco Audit, a tool that allows us to simulate various parameters such as waste production and carbon footprint, while also anticipating the economic and environmental benefits that the chosen materials would provide.

Furthermore, efforts were made to meet safety criteria for construction work, ensuring worker safety and compliance with regulations through preliminary analysis.

2. Objectives

Using Ansys Granta Edu pack, we aim to find a material for scaffolding construction that ensures the safety of workers and pedestrians, is environmentally sustainable, and remains economically competitive in the market, considering that scaffolding is widely used in civil construction.

3. Problem statement

Scaffolding is a crucial tool in civil engineering that can be assembled and placed in various ways. It must be well-structured and provide safety since it allows access to elevated locations and provides a working platform for construction workers. Consequently, it is an important structure for the progress of building's construction, which involves such influence on cost and safety of projects.[2]

Scaffolding accidents often occur due to failures at attachment points or parts, overloaded platforms, weak or defective planking, and changing environmental conditions.[3] This means that the primary material, the metal, carries risks associated with weather changes, such as humidity that can affect the pipe's resistance and increase it conductivity which is prone to electrical accidents. Another feature is the low weight, given the need to move and assemble the structure frequently,and the price. Additionally, the increase of scaffoldings raises sustainability concerns, both in terms of metal extraction, which can result in shortages in other markets and in terms of disposal.

4. Proposed solution

To meet Brazilian standards for scaffolding construction (NBR 6494), certain key conditions must be satisfied. These include having slip-resistant flooring. As a standard, scaffolding models from the European standards EN 12810-1 and EN 12810-2 were used. These models specify that the external tube diameter should be 48.3 mm, the minimum thickness should be 2.7 mm, and the maximum tube length should be around 2 meters. The total supported load for scaffolding operations involving operators, tools, and equipment is 6 kN/m2, in line with regulations.

When constructing scaffolding in Brazil, it's crucial to adhere to specific standards. These regulations dictate that the structure must maintain stability in all directions, the floors should have a rough surface to prevent slipping, and dimensions should be based on functionality. To ensure compliance, the EN 12810-1 and EN 12810-2 standards have established the European scaffold model as a reference point. This model requires a cylindrical tube with an external diameter of 48.3 mm, a minimum thickness of 2.7 mm, and a maximum length of approximately 2 m. When determining the load capacity, it's essential to take into account the weight of operators, tools, and materials. According to standards, the scaffolding must be able to support a total load of around 6 kN/m².

Therefore, with the goal of obtaining an estimate of the tension distribution, as well as the means of deformation of the scaffold structure, a static simulation was utilized, placing a vertical component of 6000 N on the cross section of each tube. In addition to that, considering maximum compression deformation of 2 mm to 4 mm, were determined, through the Solver, the parameters for the upcoming material selection process, resulting in a elastic limit of y 11,3 MPa, a Young's modulus of E 7,53 GPa and a minimum fracture toughness of 3 MPam1/2.

Subsequent to this, after applying various durability filters (Figure 1) Young's Modulus x Density Ashby Diagrams were created (Figure 2)(red curve given by Equation 1) where 57 materials reached our goals. Applying our objectives of reducing mass, cost and buckling risk, we plotted the graph of the unit of mass or buckling stiffness (Equation 1) x Cost per unit of buckling stiffness (Equation 2) (Figure

3). To achieve the best relation between these parameters, it was necessary to utilize a trade-off curve (Equation 3 with an estimated trade constant of 6.42$/Kg) given the conflicting objectives[4]. After this analysis the materials with the most optimized weight/cost are Low Alloy Steel AISI 5120; Galvanized steel; PET 35-45% Fiberglass and mica; and PET 45% fiberglass, Polymer extrusion.

In order to compare these four materials, we used the Synthesizer tool to analyze their costs and mass (Figure 4). Our findings showed that in a 50 ton package of raw material, approximately 18,315 units of the product can be produced by extrusion using PET 45% fiberglass, and that material had the lowest price and weighed only 2.73 kg per unit, making it a favorable option over the other materials.

To evaluate the environmental impact of the product package (equivalent to 50 tons of raw material) throughout its life cycle, we utilized the Eco Audit tool. Our analysis revealed that the largest contributor to energy expenditure and carbon footprint across all materials was material sourcing and manufacturing. However, PET reinforced with 45% glass fiber had lower energy consumption throughout its useful life (approximately 75 MJ) (Figure 5) and a lower carbon footprint (approximately 6 Kg) (Figure 6) compared to the other materials. In comparison to galvanized steel (500 MJ of energy and 37 Kg carbon emission), PET 45 material had a clear advantage.

As a highly implemented method in the industry to create components by compressing the material through a die, the extrusion itself is a viable process to generate cross sections of different geometries with a polymer mass mixed with fiberglass reinforcement. Analyzing the properties of these material combinations based on bubble charts and trade-off curves developed using the Limit, Solver, and Synthesizer tools, we can conclude that the most suitable material was PET 45% fiber glass with Polymer extrusion as manufacture process with optimized properties and costs had a maximum Young's Modulus equal to 14,8 GPa, a maximum density of 1,72 kg/m^3 - almost two times lower than the density of aluminum (2.7 g/cm^3)[5,6] - and a virtually zero conductivity (Figure 7).

5. Results and conclusions

The Ansys Granta EduPack software was essential in all these analyses providing a comprehensive view of the project meeting the tools requested for filtering attribute limits. The project's function, restrictive limits, objectives, and free variables were all considered, including safety while working at elevated heights, low weight, conductivity, and oxidation resistance, ease of assembly and disassembly, as well as the structure's mobility and low carbon dioxide emissions in its manufacturing process. Ultimately, polyethylene terephthalate reinforced with 45% recycled glass fibers proved to be the most advantageous option.

In addition, as observed through the Synthesizer and Eco Audit tools, the use of this material is the best ecological and financial option within the expected mechanical properties of the material and weather resistance. After all, this PET 45% fiberglass facade scaffolding is lighter and more secure for workers and pedestrians meeting all the requirements of the project.

6. References

[1] HOLA, B.; NOWOBILSKI, T.;, Rudy J.; BLAZIK, E. B.; Dangerous events related to the use of scaffolding. Technical Transactions 7/2017, Civil Engineering, 31-39.

[2] BŁAZIK-BOROWA, E.; SZER, J. The analysis of the stages of scaffolding “life” with regard to the decrease in the hazard at building works. Archives of Civil and Mechanical Engineering, v. 15, n. 2, p. 516–524, fev. 2015.

[3] ABAS, N. H.; NORIDAN, M. R.; RAHMAT, M. H.; ABAS, N. A. .; IBRAHIM, N. Q. Causes of Accidents Involving Scaffolding at Construction Sites. Journal of Technology Management and Business, [S. l.], v. 7, n. 1, p. 75–86, 2020. Disponível em: https://publisher.uthm.edu.my/ojs/index.php/jtmb/article/view/6058. Acesso em: 18 set. 2023.

[4] ASHBY, Michael. Seleção de materiais no projeto mecânico. 2019. 5th ed. Editora LTC, Brazil

[5] CÉSAR J, PAOLI M-AD, ANDRADE JC DE. A determinação da densidade de sólidos e líquidos. Rev. Chemkeys [Internet]. 17º de setembro de 2018 [citado 6º de outubro de 2023];(7):1-8. Disponível em: https://econtents.bc.unicamp.br/inpec/index.php/chemkeys/article/view/9618. Acesso em: 06 out. 2023.

[6] OLIVEIRA, J. DA C. P. T. DE .; PADILHA, A. F.. Caracterização microestrutural dos alumínios comerciais AA1100, AA1050 e AA1070 e do alumínio superpuro AA1199. Rem: Revista Escola de Minas, v. 62, n. 3, p. 373–378, jul. 2009.

7. Appendix

Equations

$$M_1 = \frac{\rho}{E^{\frac{1}{2}}} \quad (1)$$

$$M_2 = \frac{C_m \rho}{E^{\frac{1}{2}}} \quad (2)$$

$$Z = M2 + \alpha M1 \quad (3)$$

Figures

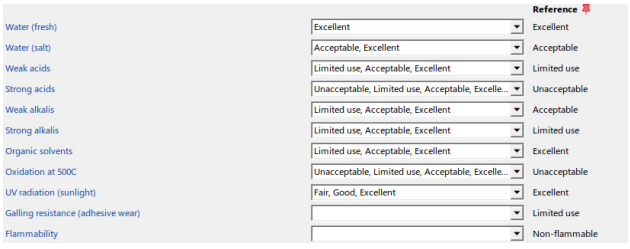

Figure 1:Applied filters in the material selection Authorial.

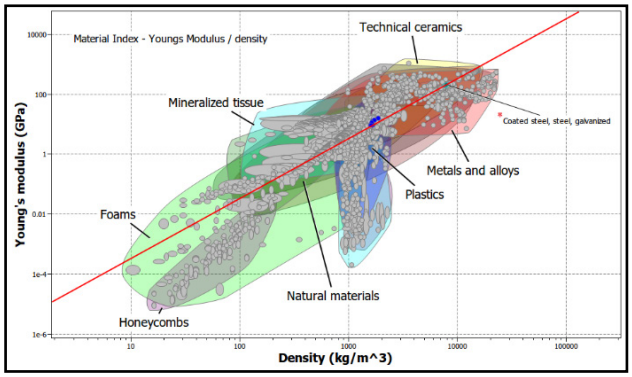

Figure 2: Screening Result + Maximization of Index M1 - 57 out of 4216 filtered materials: Authorial.

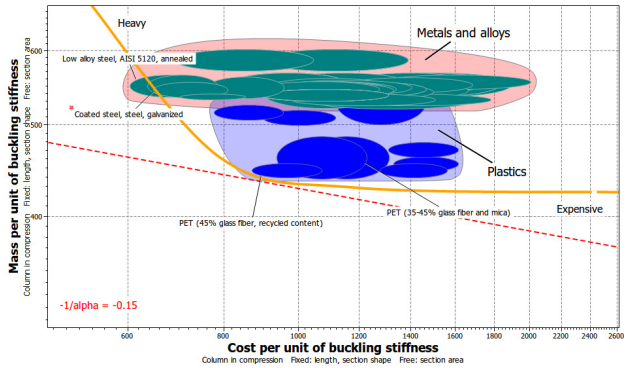

*Figure 3: Result of the plot of M1 x M2 indices with the trade-off curve Z = C + alpha * M1, where alpha is estimated at 6.42 $/kg: Authorial.*

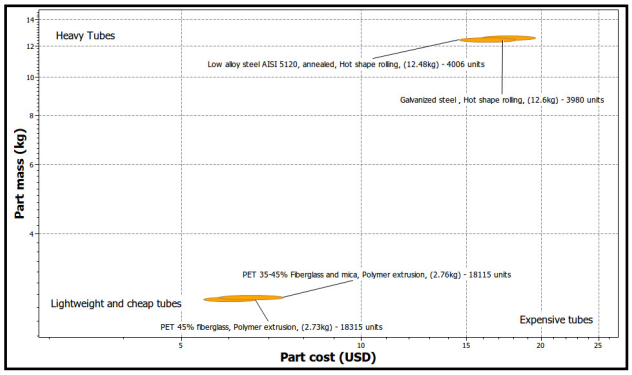

Figure 4: Price and mass estimation chart created using the Granta synthesizer to compare the final price/final mass of PET + Fiberglass pipes and the price/mass of metal pipes: Authorial.

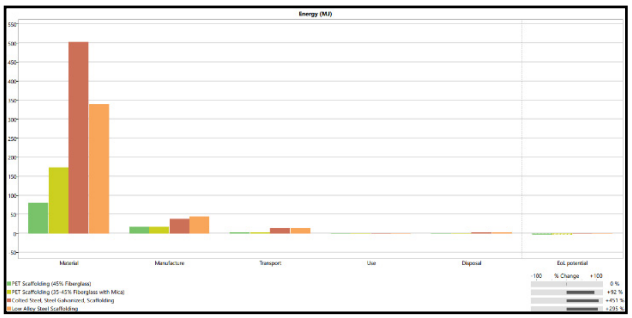

Figure 5: Eco Audit result comparing the 4 materials (considering energy): Authorial.

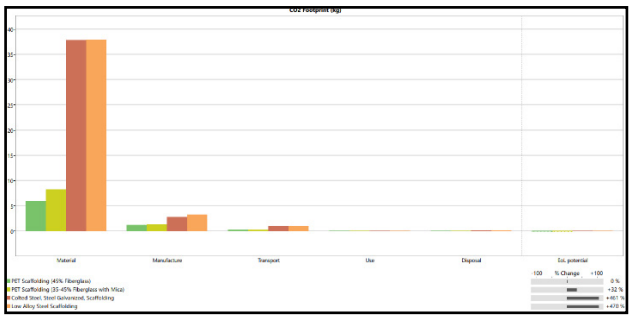

Figure 6: Eco Audit result comparing the 4 materials (considering carbon footprint): Authorial.

Electrical properties					
Electrical resistivity	ⓘ	* 3.3e20	-	3e21	µohm.cm
Electrical conductivity	ⓘ	* 5.75e-20	-	5.22e-19	%IACS
Dielectric constant (relative permittivity)	ⓘ	* 3.9	-	4.1	
Dissipation factor (dielectric loss tangent)	ⓘ	* 0.0047	-	0.0053	
Dielectric strength (dielectric breakdown)	ⓘ	20.4	-	22.1	MV/m
Comparative tracking index	ⓘ	200	-	325	V
Physical properties					
Density	ⓘ	1.68e3	-	1.72e3	kg/m^3
Mechanical properties					
Young's modulus	ⓘ	* 14.1	-	14.8	GPa
Young's modulus with temperature Parameters: Temperature = 23°C	ⓘ	14.3	-	14.3	GPa

Figure 7: Electrical, mechanical and physical properties: Databases of the Ansys Granta.

Material selection for Vertical Axis Wind Turbines

Universidade Estadual de Campinas, Limeira, Brazil

Supervisor: Alessandra Cremasco

Student/s: José Alberto Jara Quintanilla, Pedro Esch de Campos Gomes,

Macedo Víctor Roy Cáceres Huamán

Table of Contents

1. Summary

In recent years, urban centers have seen a major shift towards sustainable energy solutions to meet growing energy demands and reduce CO2 emissions. Vertical axis wind turbines such as the Darrieus, Savonius or Darrieus-Savonius are gaining popularity in urban environments due to their compact design, ability to operate in turbulent wind conditions, and aesthetic appeal [1-2]. These turbines blend easily into urban landscapes and are able to capture wind from multiple directions, making them adaptable to urban environments with complex wind patterns. However, as the demand for renewable energy continues to grow, attention is turning to offshore wind farms as a possible solution to harness the abundant wind resources in coastal regions. Offshore wind turbines present different challenges than their onshore counterpart. In marine environments, turbines are exposed to corrosive salt water, high winds and some sections to high pressures. Therefore, materials and designs that can withstand these harsh conditions need to be considered. Vertical axis wind turbines (VAWT) have emerged as a promising option for offshore installations. Unlike horizontal-axis wind turbines (HAWTs), VAWTs do not need to be precisely aligned with the wind direction, making them better suited for offshore environments where winds are more variable and turbulent. VAWTs also generate low noise and can have a low rotation speed, what makes it ideal for offshore installations as it won't damage to the marine life. The project focuses on the selection of materials for the rotor blades and structure, considering the need of excellent resistance to fatigue, salt water corrosion and high-pressure conditions, while being lightweight to facilitate installation and maintenance operations.

2. Objectives

The purpose of this project is to seek a viable material for the structure capable of withstanding the harsh conditions of saltwater and sunlight exposure, while also meeting manufacturing and recyclability requirements, considering the constraints related to the stresses involved. Within these parameters, the aim is to select a material with high fatigue resistance and low density, in order to facilitate and reduce the cost of the transportation and installation process, while also decreasing the load applied to the structure and supporting cables.

3. Problem statement

VAWT (Vertical Axis Wind Turbine) systems are highly advantageous for ocean use because they do not need to be anchored to the seabed, as they can accommodate a wide range of current directions for their rotation. Therefore, a slight tilt is not a problem; however, in this case, it is necessary to use cables that support the structure, preventing it from toppling over [3]. Furthermore, their rotation and noise levels are also low, minimizing harm to the local wildlife. However, this is a harsh environment for most materials, and transportation and installation pose significant challenges, which must be taken into account when selecting the material.

4. Proposed solution

To ensure the selection of a material suitable for the problem, it is necessary to establish some constraints. For this we used a group of parameters from a thesis entitled STUDY OF VERTICAL WIND TURBINES WITH AN EXAMPLE OF SIZING A DARREIEUS WIND TURBINE FOR BUILDING APPLICATION [4]. To ensure safety, we demand a strength of at least double the stress; thus, the following constraints were used: compressive strength of 160 MPa (minimum), fatigue strength at 10^7 cycles of 90 MPa (minimum), fracture toughness of 60 MPa/$m^{1/2}$ (minimum), maximum operating temperature of 100°C (minimum), minimum operating temperature of -40°C (maximum), excellent casting and welding capabilities, as well as excellent durability in saltwater and sunlight environments. Lastly, it must also be non-biodegradable while it is recyclable. This way, we can ensure that the material will be capable of performing in any region of the planet.

5. Results and conclusions

As a result, we obtained a small range of possibilities, including CuSn9Pb1 bronze, C52400 cast (phosphor bronze), titanium commercial purity grade 1, and titanium commercial purity grade 2, among which the top choices are CuSn9Pb1 bronze, C52400 cast (phosphor bronze), and titanium commercial purity grade 2. The first offers a significant cost advantage, while the second has significantly lower density and higher fatigue resistance. Thus, there is a tendency to define titanium as the best choice due to its greater durability and potential reduction in the structure's dimensions. However, in specific cases, bronze may be more attractive for financial reasons.

6. References

[1] Kumar, R. Raahemifar, K. Fung , A. Critical review of vertical axis wind turbines for urban applications
[2] Ragheb, M. VERTICAL AXIS WIND TURBINES
[3] Xu, W. Li, G.; Li, Y. Feasibility analysis of aerodynamic characteristics for vertical-axis turbines in offshore: A comprehensive analysis on scale and design of wind system
[4] Purificação, L. Fonte, R.ESTUDO DE TURBINAS EÓLICAS VERTICAIS COM EXEMPLO DE DIMENSIONAMENTO DE UMA TURBINA EÓLICA DARRIEUS PARA APLICAÇÃO EM EDIFÍCIOS

7. Appendix

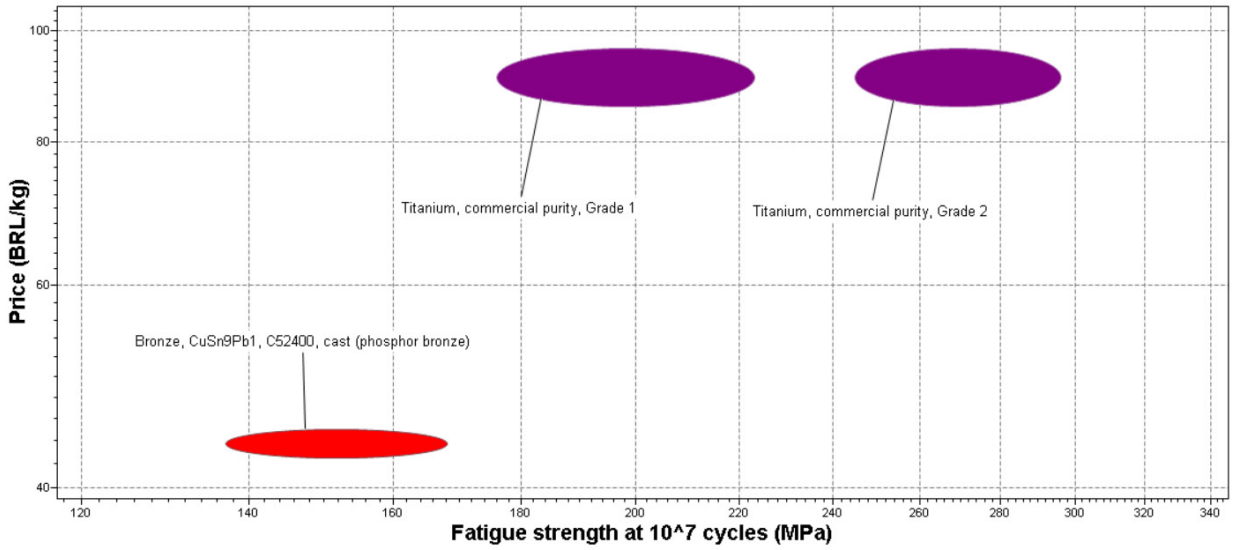

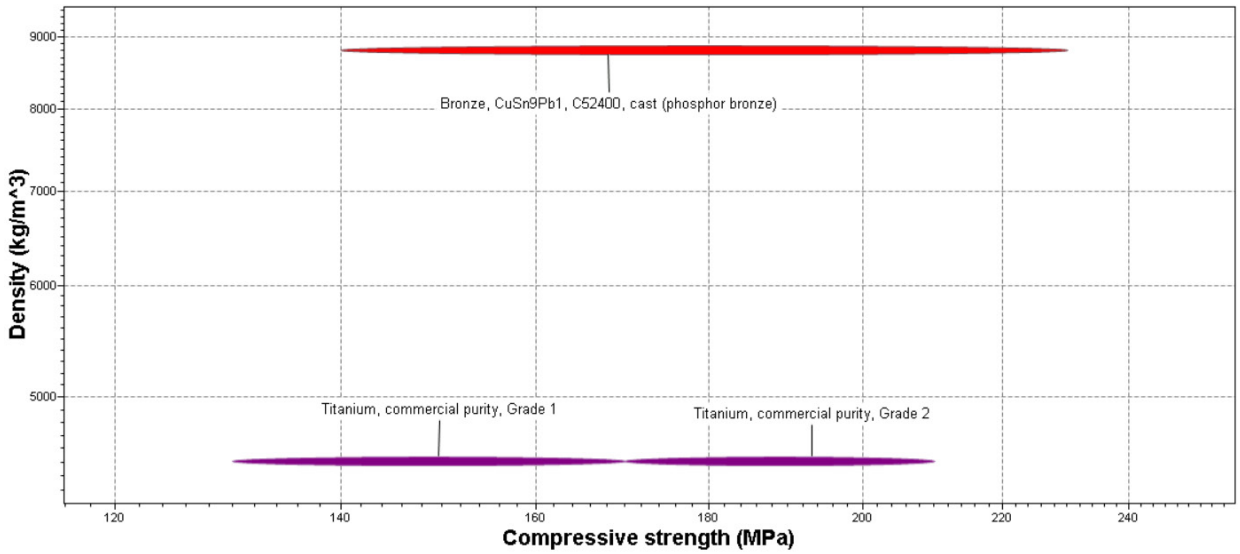

Multilayer material for the Whipple shield front bumper of human transportation spacecrafts with a thermal isolation additional improvement.

Polytechnical University of Madrid (UPM), Madrid, Spain

Supervisor: Sandra Tarancón Román

Student/s: Aida Martínez Barja

Report Contents

1. Summary

Due to the growing research interest about interplanetary human travelling and the possibility of inhabiting other planets, the amount of space debris is increasing sharply [1]–[3]. To protect the space vehicles from the impact of this space debris or even of micrometeorites at hypervelocity of 3 – 18 km/s [4], Whipple shields are used in some critical parts of the spacecrafts, and consist of a front bumper and a spaced rear wall [5], scheme on Figure 1a. The projectile first impacts the bumper enduring an acute fragmentation and a phase change, conforming the called debris cloud behind the bumper, which diffusion degree determines the rear plate damage [1]. Since the Whipple shield invention in 1940 by Fred Whipple [4], different materials and strategies have been used for this structure. The most common and first material used was aluminum [4], [5]. Then some experiments were performed to improve its performance, using impedance graded multilayer materials [6]–[9], using stuffed [2] or multi-shock Whipple as well as composite materials [10] with intercalated layers of

foam [11], [12], reactive materials [3], amorphous alloys [13] or self-healing ionomer materials [14]. Also, the possibility of filling the gap between the bumper and the rear plate with high pressure gas has been explored [1]. In this project it was decided to design an impedance-graded Whipple shield, based on its higher capability of breaking the projectile in smaller fragments when colliding [6]–[9]. This is due to the combination of the reflections and transmissions of the shock wave produced in the collision, resulting from the impedance mismatch. Consequently, tensile and compression stresses are produced in different directions of the projectile, breaking it. Moreover, it was decided to add one layer for improving thermal isolation. The Synthesizer tool of GRANTA EduPack was deeply used for designing the different composite materials that integrate the final multilayer.

2. Objectives

The objective of the Whipple shield front bumper is to break the projectile in the smallest fragments as possible or to decompose it, to reduce the damage in the rear plate or in the spacecraft skin. Therefore, the main objective of this project is to design and select the materials to create an impedance graded multilayer bumper. A secondary objective is to improve the thermal isolation of the multilayer, hence reducing costs in the spacecraft thermal control subsystems.

3. Problem statement

Design an impedance-graded multilayer material to be used as the front bumper of a Whipple shield for spacecraft protection against hypervelocity collisions in the space. Moreover, one of the layers should suppose an additional improvement in thermal isolation. To simplify the problem and the material selection, some initial statements were established about the material subtype used on each layer, based on referenced arguments numbered below:

1) The multilayer will have 4 layers
2) The1st (outer layer) and 3rd layer will be composed of the same bulk metal (material 1) [4].
3) The 2nd layer (material 2) is going to be composed for a metal matrix composite (MMC) reinforced with ceramic particles.

Because using MMC reinforced with ceramic particles: the Young's modulus (E), density (ρ) and therefore the acoustic impedance (Z) is going to be higher than when using a bulk metal, thus establishing a Z gradient with material 1. Also having the advantages of using an MMC: the hardness of the ceramic particles but with the ductility and toughness of the metallic matrix [5]. Furthermore, it was considered that having very small and hard particles distributed in a metallic matrix will help in the projectile fragmentation. As the MMC will be designed to have higher ρ than the material 1 (to stablish the Z gradient), is better to use it only in the 2nd layer and the bulk metal in the 1st and 3rd layers, to have a lighter multilayer. 4) The 4th layer (material 3, inner layer) will be a low-density thermal insulation closed-cell polymeric foam. Because closed-cell polymeric foams are among the materials with lower thermal conductivity (λ) and have lower λ than open-cell foams [15] while maintaining a very low ρ [16]. This layer must improve thermal isolation without supposing an extra weight in the total multilayer material.

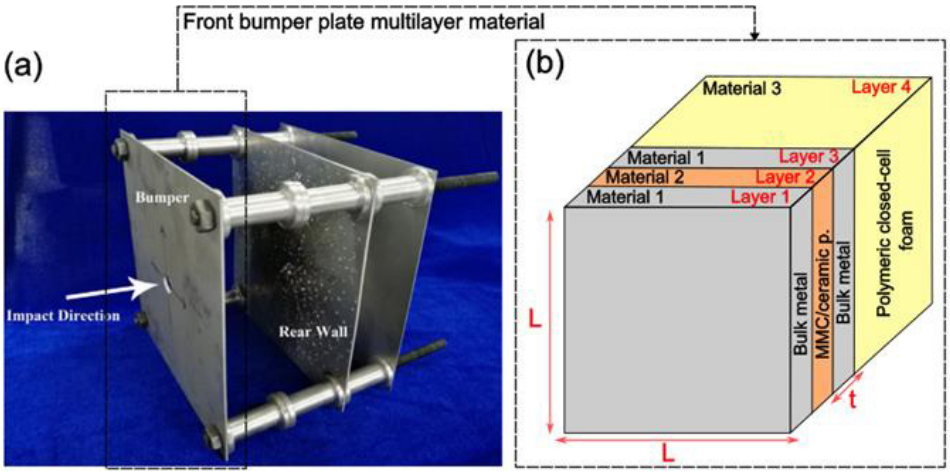

Figure 1. (a) Specimen of a Whipple shield after impact test, showing its main parts: front bumper, spaced rear wall and "spacecraft skin" final layer [5]. (b) Scheme of the proposed multilayer material design with its layers and the subtype material pre-defined for each of them.

A scheme of the multilayer proposed is shown in Figure 1b. For the calculations: each layer is considered a cubic prism, with lateral dimensions "L" and thickness "t". The materials will be selected using GRANTA EduPack software – Level 3 Aerospace database. To design the MMC, the foam, and the final multilayer, the Synthesizer tool will be used.

4. Proposed solution

Is very difficult to calculate or simulate the mechanical properties that the shield material should possess because the objects that could collide with the spacecraft have very different shapes and sizes [4] , and the impact velocity has a wide range. The possible loads for all the possible impacts the material could suffer cannot be calculated. Hence, to simplify the problem and to be able to perform the material selection, it was decided to base the mechanical properties restrictions in the ones of the aluminum alloy Al 2024, T6. Because Al alloys has been widely used for this purpose since the beginning [4] [5], and this is one of the most famous Al aerospace alloys. To solve the problem, first: define the constraints (C) and objectives for each of the layers. Then, using the objective functions (OF) in combination with C: calculate and apply the material indexes (MI) to rank the materials. In Table 1 of Appendix (Ap) A is the summary of all the C, OF and MI used. The calculations performed are in Ap B. The dimensions and the total mass of this part of the Whipple shield is very difficult to establish. Because these structures are used in some critical parts of the spacecraft, and their mass and dimensions vary a lot in terms of the space vehicle type. Therefore, it was impossible to stablish a mass restriction. The procedure followed to select the material of each layer is described below:

4.1 Material 1 (subindex "1").

It will be a bulk metal. The constraints regarding its mechanical properties are based on Al 2024, T6, so: C1, C2, C3 and C4. Regarding the thermal properties, if the shield material temperature increases notably with the impact, it will help in the projectile melting or decomposition [6]. In addition, if the shield melts, it could help to stop the projectile or to the hole closing after the impact (like self-repairing). Hence, materials with a lower specific heat are preferred, because are easier to be heated by the impact: C5. This material will be in contact with the atmosphere, so it need to support the T range of the space: C6 [17], and be resistant to UV radiation: C7. For safety reasons it should be non-flammable or self-extinguish: C8. The thickness of the layer is restricted to 0,5 mm: C9, to match with

the literature values [8]. The objectives set was to maximize λ: OF1 (to allow the heat conduction from the shield to the projectile), minimize the mass: OF2 (is part of a flying vehicle), and maximize the T increase in the collision: OF3.

4.2 Material 2 (subx. "2")

It will be a MMC reinforced with ceramic particles. First, the material for the matrix (subx. "m2") will be selected, which is a metal. The constraints for the matrix are C1, C2, C3, C4, C5, C6 and C8 for the same reason as for material 1, and C10 to establish the impedance mismatch. Then, the material selection for the ceramic particles (subx. "p2"), using C11, because we want a material harder than the matrix. For the final MMC, the constraint is C9, the objectives are OF1, OF2, OF3 and OF4, and for ranking the materials, MI-1 and MI-2 will be used.

4.3 Material 3

It will be a polymeric closed-cell foam. Its constraints are C12 and C13 to ensure its thermal isolation ability without suppose an extra weight. The objective will be OF2, and to rank the materials, MI-3 will be used.

4.4 Final multilayer

The only magnitude that seems to be well estimated by Synthesizer for multilayers is ρ and maybe E. Therefore, the defined constrained was C1, as objective OF2, and to rank the materials: MI-4.

5. Results and conclusions

This section includes the description of the selection process followed using GRANTA EduPack, briefly commenting the obtained results. All the graphs obtained in GRANTA that are referenced in the text are included in Ap C.

5.1 Selection of Material 1 (1st and 3rd layer)

(1a) Inside the metals and alloys subset
(1b) a limit stage with C1, C2, C3, C4, C5, C6, C7, C8 was applied. The 251 materials that passed
(1c) were ranked with MI-1, Figure 2. Although the better ones were Ag and Pd alloys, due to its high cost, the material finally chosen was: *Aluminum, 2024, T861*.

5.2 Selection of Material 2 matrix.

(2a) Inside the metals and alloy subset
(2b) a limit stage with C1, C2, C3, C4, C5, C6 and C8 was applied; and 251 materials passed.
(2c) To apply C10, Z1 must be calculated (using the units of GRANTA in the graphs), that for the selected material was:

$$Z_1 = \sqrt[2]{\rho_1 \cdot E_1} = \sqrt[2]{2780\,\frac{\mathrm{kg}}{\mathrm{m^3}} \cdot 75\ \mathrm{GPa}} \approx 457\sqrt[2]{\frac{\mathrm{kg \cdot GPa}}{\mathrm{m^3}}}$$

Therefore, C10 results:

$$Z_2 > 685^2\sqrt{\frac{kg \cdot GPa}{m^3}}$$

(2d) Applying this limit in a $^2V\rho_1 \cdot E_1$ graph, Figure 3, three materials that are over this value and that are economically affordable were chosen: *Cobalt-base superalloy, L605, solution treated ; Copper-berylium alloy, CuBe2, C17200, TH04 and Titanium, near-alpha alloy, Ti-6Al-5Zr-0.5Mo.*

5.3 Selection of Material 2 particles

(3a) Inside the ceramic and glasses subset
(3b) a limit stage with C11 was applied, that was HV_{p2}*>440 HV* for the most restrictive case. 117 materials passed and
(3c) were ranked in terms of hardness and density, Figure 4, rejecting diamond by its price and WC by its weight so selecting: *B4C and SiC.*

5.4 Selection of Material 2 (2nd layer)

(4a) All the possible combinations of MMC reinforced with particles using the previously selected materials were created with Synthesizer.
(4b) Applying MI-1 the better materials were: $CuBe_2$ matrix - SiC 70% fv reinforced and $CuBe_2$ matrix - B_4C 30% re., Figure 5. However, when
(4c) applying MI-2, the better materials were Co superalloy SiC 30% re. and Co superalloy B_4C 30% re., Figure 6.
(4d). Finally, the better one of each MI was selected: *$CuBe_2$ - SiC 70%. and Co - SiC 30%.*
(4e) Then, the multilayer with the first 3 layers was created, because it is needed to calculate its ρ for then selecting Material 3. The impedance mismatch achieved between material 1 and 2 has the value of $R=Z_2/Z_1=2.46$ with $CuBe_2$ matrix and $R=3.14$ with Co matrix.

5.5 Selection of Material 3 (4th layer)

(5a) Definition of a subset with the most common polymers used as a rigid foam: PS, PP, PU, PE and PF and
(5b) ranking them by its λ. The ones with lower λ were PS, PP and PVC so close-cell foams with them were created in the Synthesizer.
(5c) After a limit stage with C12 and C13: $\rho \leq 170$ kg/m^3 , 6 of the 9 manufactured foams passed.
(5d) Classifying by MI-3 (Figure 7), *PS (0,01) and PP (0,011) foams* were selected.

5.6 Selection of the final multilayer

(6a) All the possible multilayer combinations were created with Synthesizer, defining a thickness of 0,5 mm for each layer to avoid problems with the properties estimations, although the fourth layer is intended to occupy the entire gap between the front bumper and the rear wall in the real application. The combinations of 1st/2nd/3rd /4th layer were the following: Al 2024 T861/Co-SiC 30%/Al 2024 T861/PP foam; Al 2024 T861/Co-SiC 30%/Al 2024 T861/ PS foam; Al 2024 T861/$CuBe_2$-SiC 70%/Al 2024 T861/PP foam and Al 2024 T861/$CuBe_2$ -SiC 70%/ Al 2024 T861/PS foam.
(6b) Ranking these 4 materials using MI-4, Figure 8: the E difference between the multilayer with Co matrix and the one with $CuBe_2$ matrix was of only 2 GPa. However, the difference in ρ is greater so its better to use the lighter multilayer: with $CuBe_2$-SiC 70%. The type of foam used did not change E or ρ, so
(6c) PS and PP foams already registered in the GRANTA database were compared using the comparison tool. The PP foam is cheaper and has, on average, lower environmental impact. Hence, the final selected multilayer material was: *Al 2024 T861 / $CuBe_2$ matrix - SiC 70% fv reinforced / Al 2024 T861 / PP foam (0,011)*. Its properties are summarized in Table 2, Ap C.

6. References

[1] K. Wen, X. wei Chen, and Y. gang Lu, “Research and development on hypervelocity impact protection using Whipple shield: An overview,” Defence Technology, vol. 17, no. 6. China Ordnance Industry Corporation, pp. 1864–1886, Dec. 01, 2021. doi: 10.1016/j.dt.2020.11.005.

[2] F. wei Ke, S. yu Zou, K. Wen, Q. Luo, X. zhong Wen, and J. Huang, “The influences of interface effect of stuffed layer on the performance of improved Whipple shields,” Int J Impact Eng, vol. 177, Jul. 2023, doi: 10.1016/j.ijimpeng.2023.104579.

[3] S. Ren et al., “Impact resistance mechanism of reactive material bumper for spacecraft Whipple shield: Experiments and numerical simulations,” Aerosp Sci Technol, vol. 126, Jul. 2022, doi: 10.1016/j.ast.2022.107646.

[4] A. Pai, R. Divakaran, S. Anand, and S. B. Shenoy, “Advances in the Whipple Shield Design and Development:: A Brief Review,” Journal of Dynamic Behavior of Materials, vol. 8, no. 1. Springer Science and Business Media Deutschland GmbH, pp. 20–38, Mar. 01, 2022. doi: 10.1007/s40870-021-00314-7.

[5] X. Huang et al., “Hypervelocity impact damage behavior of B4C/Al composite for MMOD shielding application,” Mater Des, vol. 186, Jan. 2020, doi: 10.1016/j.matdes.2019.108323.

[6] P. L. Zhang et al., “Study of the shielding performance of a Whipple shield enhanced by Ti-Al-nylon impedance-graded materials,” Int J Impact Eng, vol. 124, pp. 23–30, Feb. 2019, doi: 10.1016/j.ijimpeng.2018.08.005.

[7] S. Ren, R. Long, Q. Zhang, and C. Chen, “The hypervelocity impact resistance behaviors of NbC/Al2024 ceramic-metal composites,” Int J Impact Eng, vol. 148, Feb. 2021, doi: 10.1016/j.ijimpeng.2020.103759.

[8] P. Zhang et al., “Comparison of shielding performance of Al/Mg impedance-graded-material-enhanced and aluminum Whipple shields,” Int J Impact Eng, vol. 126, pp. 101–108, Apr. 2019, doi: 10.1016/j.ijimpeng.2018.12.007.

[9] A. J. Stilp and K. Weber, “DEBRIS CLOUDS BEHIND DOUBLE-LAYER TARGETS,” 1997.

[10] M. Higashide, T. Kusano, Y. Takayanagi, K. Arai, and S. Hasegawa, “Comparison of aluminum alloy and CFRP bumpers for space debris protection,” in Procedia Engineering, Elsevier Ltd, 2015, pp. 189–196. doi: 10.1016/j.proeng.2015.04.026.

[11] E. K. Stansbery, “Shield Development,” https://hvit.jsc.nasa.gov/shield-development/.

[12] A. Klavzar, M. Chiroli, A. Jung, and B. Reck, “Protective performance of hybrid metal foams as MMOD shields,” in Procedia Engineering, Elsevier Ltd, 2015, pp. 294–301. doi: 10.1016/j.proeng.2015.04.050.

[13] X. Huang, Z. Ling, Z. D. Liu, H. S. Zhang, and L. H. Dai, “Amorphous alloy reinforced Whipple shield structure,” Int J Impact Eng, vol. 42, pp. 1–10, Apr. 2012, doi: 10.1016/j.ijimpeng.2011.11.001.

[14] A. Francesconi et al., “Comparison of self-healing ionomer to aluminium-alloy bumpers for protecting spacecraft equipment from space debris impacts,” Advances in Space Research, vol. 51, no. 5, pp. 930–940, Mar. 2013, doi: 10.1016/j.asr.2012.10.013.

[15] A. M. S. SUR-SEAL, “WHY YOU SHOULD USE CLOSED-CELL FOAM,” https://www.sur-seal.com/blog/why-you-should-use-closed-cell-foam/#:~:text=Closed%2Dcell%20foam%20will%20not,foam%20is%20its%20water%20resistance.

[16] M. Santiago-Calvo, J. Tirado-Mediavilla, J. L. Ruiz-Herrero, F. Villafañe, and M. Á. Rodríguez-Pérez, “Long-term thermal conductivity of cyclopentane–water blown rigid polyurethane foams reinforced with different types of fillers,” Polym Int, vol. 68, no. 10, pp. 1826–1835, Oct. 2019, doi: 10.1002/pi.5893.

[17] Angela Libal, “The Temperatures of Outer Space Around the Earth,” https://sciencing.com/temperatures-outer-space-around-earth-20254.html.

7. Appendix

Appendix A: Summary table of constraints, objectives and materials indexes

Table 1. Summary of all the constraints (C), objective functions (OF) and material indexes (MI) used in the selection process

CONSTRAINTS		OBJECTIVE FUNCTIONS		MATERIAL INDEXES	
C1	$E \geq E_{2024,T6} = 75\ GPa$	**OF1**	Maximize λ $\lambda = \frac{qt}{\Delta T}$	**MI-1**	C5+OF1+OF2+OF3 $\frac{\lambda}{\rho C_p} \geq \frac{L^2 t^2 q}{Q}$
C2	$\sigma_y \geq \sigma_{y_{2024,T6}} = 380\ MPa$				
C3	$K_{IC} \geq K_{IC_{2024,T6}} = 40\ MPa\sqrt[2]{m}$				
C4	$G \geq G_{2024,T6} = 22\ kJ/m^2$	**OF2**	Minimize mass "m" $m = \rho V = \rho L^2 t$	**MI-2**	C10+OF4 $Z_2 > \sqrt[2]{\rho_1 \cdot E_1}$
C5	$C_p \leq C_{p_{2024,T6}} = 880\ J/kg\ ^0C$				
C6	T range = (-270 °C, 600 °C)	**OF3**	Maximize the T increase produced during the impact $\Delta T = \frac{\beta}{\rho C_p}\int_0^{\varepsilon_f} \sigma d\varepsilon$ $\Delta T \propto 1/\rho C_p$	**MI-3**	C12+OF2 $\lambda \cdot \rho \leq \frac{qm}{L^2 \Delta T}$
C7	Resistance to UV radiation = Good, Excellent				
C8	Non-flammable, self-extinguish				
C9	$t = 0{,}5\ mm$				
C10	$Z_2 > 150\%\ Z_1 \rightarrow \rho_{m2} > \rho_1, E_{m2} > E_1$				
C11	$HV_{p2} > HV_{m2}$	**OF4**	Maximize Z_2 $Z_2 = \sqrt[2]{\rho_2 \cdot E_2}$	**MI-4**	C1+OF2 $\frac{E}{\rho} \geq \frac{Ft^2}{\Delta t m}$
C12	$\lambda \leq 0{,}03\ W/(m\ ^0C)$				
C13	$\rho \leq 5\ \%\ \rho_{layers1+2+3}$				

Appendix B: Calculations and equations

B1) Acoustic impedance equation

$$Z = \rho \cdot c = \rho \cdot \sqrt[2]{E/\rho} = \rho \cdot E^{\frac{1}{2}} \cdot \rho^{-\frac{1}{2}} = \rho^{\frac{1}{2}} \cdot E^{\frac{1}{2}} = \sqrt[2]{E \cdot \rho}$$

B2) Material indexes calculations

MI-1 = C5 $\left(C_p \leq C_{p_{2024,T6}} = 880\ J/kg\ ^0C\right)$ + OF1 $\left(\lambda = \frac{qt}{\Delta T}\right)$ + OF2 $\left(m = \rho L^2 t\right)$ + OF3 $\left(\Delta T \propto 1/\rho C_p\right)$

$$C_P \leq \frac{Q}{m\Delta T} \rightarrow OF1\ \left(\Delta T = \frac{qt}{\lambda}\right) \rightarrow C_P \leq \frac{Q}{m\frac{qt}{\lambda}} \rightarrow \frac{C_P}{\lambda} \leq \frac{Q}{mqt} \rightarrow OF2\ \left(m = \rho L^2 t\right) \rightarrow \frac{C_P}{\lambda} \leq \frac{Q}{\rho L^2 tqt} \rightarrow \frac{\rho \cdot C_P}{\lambda} \leq \frac{Q}{L^2 qt^2}$$

$$MI - 1 \rightarrow \frac{\lambda}{\rho \cdot C_P} \geq \frac{L^2 qt^2}{Q}$$ (OF3 is implicit in the equation)

MI-2 = C10 $\left(Z_2 > 150\%\ Z_1\right)$ + OF4 $\left(Z_2 = \sqrt[2]{\rho_2 \cdot E_2}\right)$

$$MI - 2 \rightarrow Z_2 > 150\%\ \sqrt[2]{\rho_1 \cdot E_1}$$

MI-3 = C12 $\left(\lambda \leq 0{,}03\ W/(m\ ^0C)\right)$ + OF2 $\left(m = \rho L^2 t\right)$

$$\lambda \leq \frac{qt}{\Delta T} \rightarrow OF2\ \left(t = \frac{m}{L^2 \cdot \rho}\right) \rightarrow \lambda \leq \frac{q\frac{m}{L^2 \cdot \rho}}{\Delta T} \rightarrow \lambda \cdot \rho \leq \frac{qm}{\Delta T \cdot L^2}$$

$$MI - 3 \rightarrow \lambda \cdot \rho \leq \frac{qm}{\Delta T \cdot L^2}$$

MI-4 = C1 $\left(E \geq E_{2024,T6} = 75\ GPa\right)$ + OF2 $\left(m = \rho L^2 t\right)$

$$E \geq \frac{\sigma}{\varepsilon} = \frac{\frac{F}{A}}{\frac{\Delta t}{t}} = \frac{\frac{F}{L^2}}{\frac{\Delta t}{t}} = \frac{F \cdot t}{L^2 \cdot \Delta t} \rightarrow OF2\ \left(L^2 = \frac{m}{t \cdot \rho}\right) \rightarrow E \geq \frac{F \cdot t}{\frac{m}{t \cdot \rho} \cdot \Delta t} = \frac{F \cdot t^2 \cdot \rho}{m \cdot \Delta t}$$

$$MI - 4 \rightarrow E/\rho \geq \frac{F \cdot t^2}{m \cdot \Delta t}$$

Appendix C: Graphs obtained during the selection process and table with the final multilayer properties

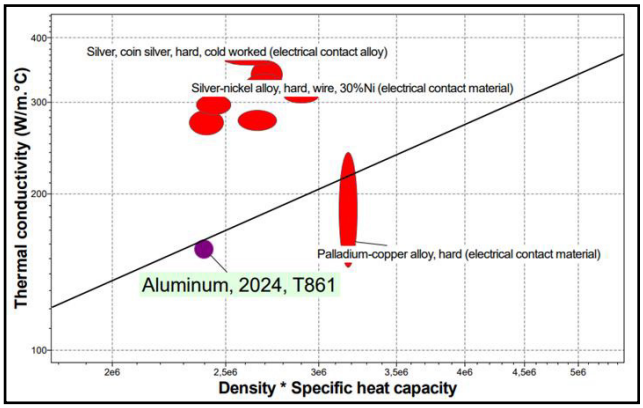

Figure 2. Graph after applying MI-1 for selecting the Material 1 for the 1st and 3rd layers. The chosen material is highlighted.

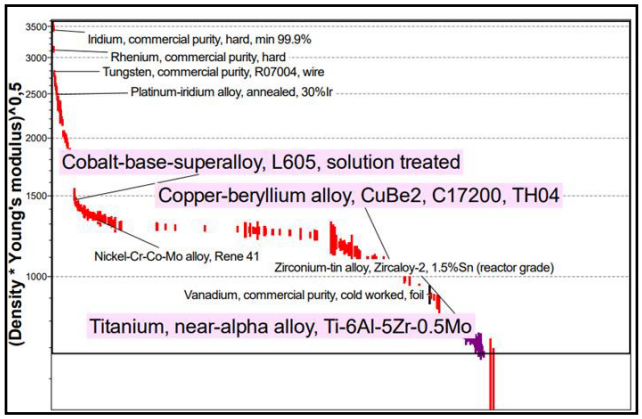

Figure 3. Graph after applying C10 for selecting the matrix of Material 2. The chosen materials are highlighted.

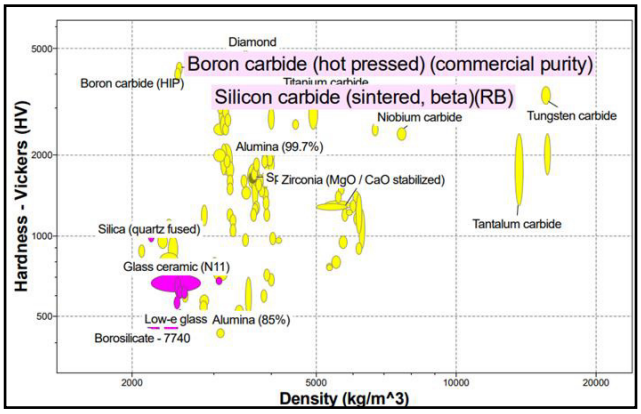

Figure 4. Graph comparing hardness and density of the possible ceramics to use as reinforcement particles in Material 2. The chosen materials are highlighted.

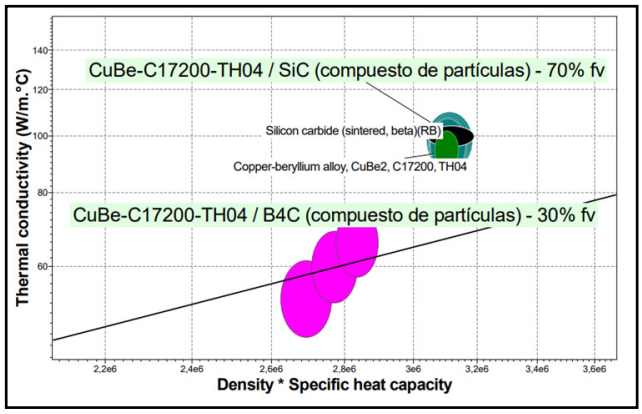

Figure 5. Graph after applying MI-1 for selecting Material 2 (2nd layer). The better materials are highlighted.

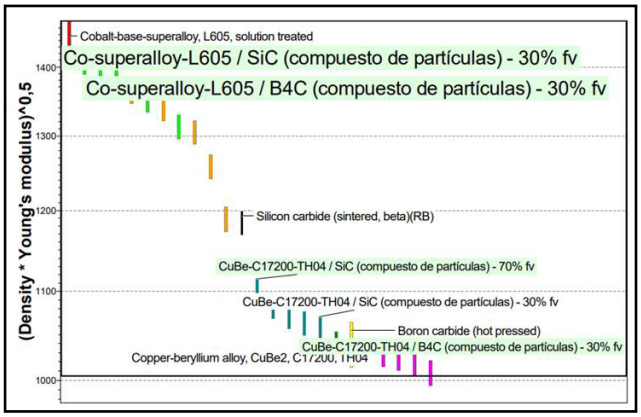

Figure 6. Graph after applying MI-2 for selecting Material 2 (2nd layer). The better materials are highlighted in bigger letters.

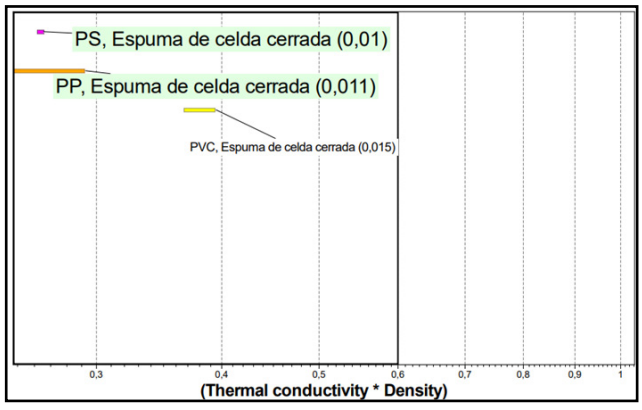

Figure 7. Graph after applying MI-3 for selecting Material 3 (4th layer). The better materials are highlighted.

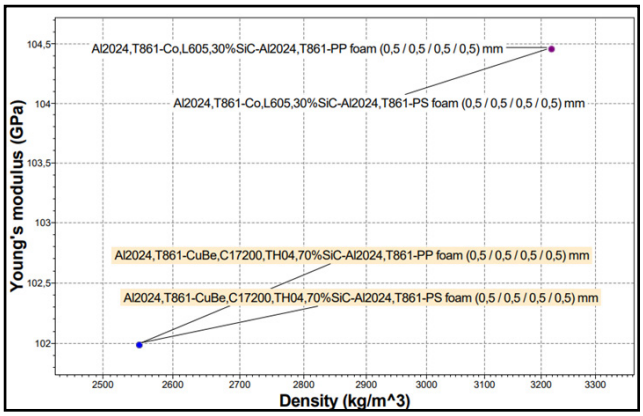

Figure 8. Graph after applying MI-4 for selecting the final multilayer. The better materials regarding density are highlighted.

Table 2. Summary of properties of the final multilayer. Defining layers with a thickness of 0.5 mm. These values are estimated by the Synthesizer tool, but some errors could exist due to the assumptions and simplifications made by the software.

$\rho\ (kg/m^3)$	$2{,}55\ \times 10^3$
$E\ (GPa)$	102
$\sigma_y\ (MPa)$	103
$\lambda\ (W/(m^0C))$	0,101
$C_P\ (J/(kg^0C))$	776

Note: In the case of this project the properties of the final multilayer are not the most important. Because the objectives were set specifically for each layer, and the important are the properties of each selected layer, the impedance mismatch between the layers, and the low thermal conductivity and density of the 4th layer. Look at the properties of the complete multilayer do not help to evaluate the final decision of the chosen material.

Appendix D: Synthesizer tool

MMC creation

Particulate reinforced composites tool. Software suppositions: Uniform size and distribution of the particles. Perfect adhesion between matrix and particles. Total dense material. The parameters used when creating the materials: % fv of particles = 30 -70, with 5 values.

Foam creation

Cellular structures – Closed cell foam tool. Software suppositions: Cell structure and size is uniform. Isotropic cell geometry. The parameters used: relative density = 1-25%, with 3 values; % material in the faces = 20%; λ_{gas}*=0.025 W/(m°C)*; defect relative size = 10.

Multilayer creation

Multilayer material 3- and 4-layers tool. Software suppositions: perfect adhesion between layers, load applied on the outer surface. Parameters used: layer thickness = 0,05 mm.

Use and Reproduction

The content used in this resource may only be used or reproduced for teaching purposes; and any commercial use is strictly prohibited.

Document Information

This report is the culmination of work for the 2022 Materials Selection Challenge held in Iberia and the Americas.

Ansys Education Resources

To access more undergraduate education resources, including lecture presentations with notes, exercises with worked solutions, microprojects, real life examples and more, visit www.ansys.com/education-resources.

Feedback

If you notice any errors in this resource or need to get in contact with the authors, please email us at education@ansys.com.

ANSYS, Inc.
Southepointe
2600 Ansys Drive
Canonsburg, PA 15317
U.S.A.
724.746.3304
ansysinfo@ansys.com